Accepted Manuscript

Cink4T, a quinazolinone-based dual inhibitor of Cdk4 and tubulin polymerization, identified via ligand-based virtual screening, for efficient anticancer therapy

Vinay Sonawane, Mohd Usman Mohd Siddique, Surender Singh Jadav, Barij Nayan Sinha, Venkatesan Jayaprakash, Bhabatosh Chaudhuri

PII: S0223-5234(19)30017-0

DOI: https://doi.org/10.1016/j.ejmech.2019.01.011

Reference: EJMECH 11018

To appear in: *European Journal of Medicinal Chemistry*

Received Date: 18 October 2018

Revised Date: 5 January 2019

Accepted Date: 5 January 2019

Please cite this article as: V. Sonawane, M.U. Mohd Siddique, S.S. Jadav, B.N. Sinha, V. Jayaprakash, B. Chaudhuri, Cink4T, a quinazolinone-based dual inhibitor of Cdk4 and tubulin polymerization, identified via ligand-based virtual screening, for efficient anticancer therapy, *European Journal of Medicinal Chemistry* (2019), doi: https://doi.org/10.1016/j.ejmech.2019.01.011.

Graphical Abstract

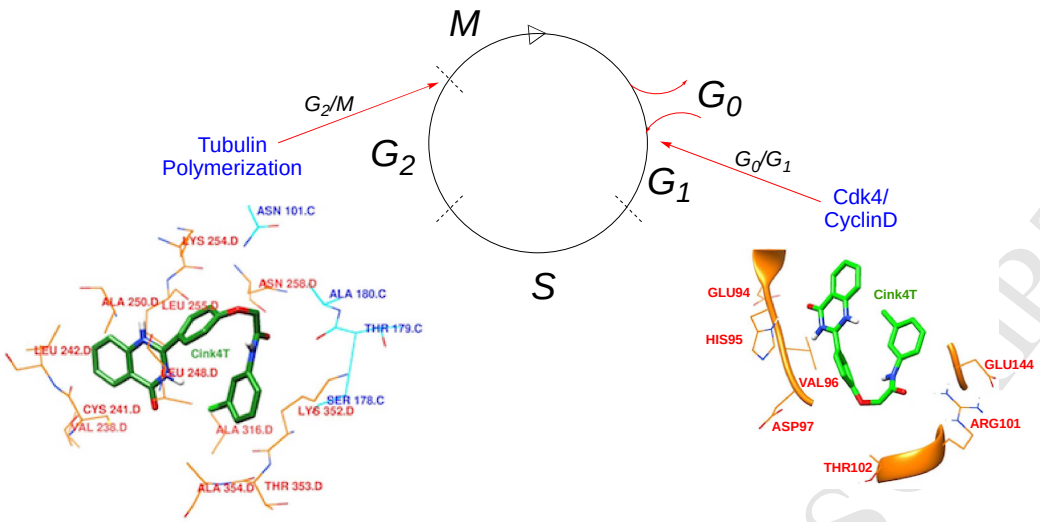

Cink4T, a quinazolinone-based dual inhibitor of Cdk4 and tubulin polymerization, identified via ligand-based virtual screening, for efficient anticancer therapy

Vinay Sonawane,[a, †] Mohd Usman Mohd Siddique,[b, †] Surender Singh Jadav,[c] Barij Nayan Sinha,[b] Venkatesan Jayaprakash,[b,*] Bhabatosh Chaudhuri[a,*]

[a]Leicester School of Pharmacy, De Montfort University, Leicester, LE1 9BH, UK

[b]Department of Pharmaceutical Sciences Technology, Birla Institute of Technology, Mesra, Ranchi 835215, India

[c]CSIR-Indian Institute of Chemical Technology, Tarnaka, Hyderabad 500007, India

[†] Contributed equally to this work.

* Authors for correspondence.

Venkatesan Jayaprakash (VJ): Email: venkatesanj@bitmesra.ac.in; Tel: +91-9470137264

Bhabatosh Chaudhuri (BC): Email: bchaud00@gmail.com; Tel: 00-44-7805230121

Declaration of interest: None

Abstract

Inhibition of cyclin dependent kinase 4 (Cdk4) prevents cancer cells from entering the early G_0/G_1 phase of the cell division cycle whereas inhibiting tubulin polymerization blocks cancer cells' ability to undergo mitosis (M) late in the cell cycle. We had reported earlier that two non-planar and relatively non-toxic fascaplysin derivatives, an indole and a tryptoline, inhibit Cdk4 with IC_{50} values of 6.2 and 10 µM, respectively. Serendipitously, we had also found that they inhibited tubulin polymerization. The molecules were efficacious in mouse tumor models. We have now identified Cink4T in a 59-compound quinazolinone library, designed on the basis of ligand-based virtual screening, as a compound that inhibits Cdk4 and tubulin. Its IC_{50} value for Cdk4 inhibition is 0.47 µM and >50 µM for inhibition of Cdk1, Cdk2, Cdk6, Cdk9. Cink4T inhibits tubulin polymerization with an IC_{50} of 0.6 µM. Molecular modelling studies on Cink4T with Cdk4 and tubulin crystal structures lend support to these observations. Cancer cell cycle analyses confirm that Cink4T blocks cells at both G_0/G_1 and M phases as it should if it were to inhibit both Cdk4 and tubulin polymerization. Our results show, for the very first time, that virtual screening can be used to design novel inhibitors that can potently block two crucial phases of the cell division cycle.

Keywords: Quinazolinone; Dual inhibitor; Cdk4; Tubulin polymerization; G_0/G_1 arrest; G_2/M arrest

1. Introduction

Cyclin-dependent kinases (Cdks) are serine/threonine-specific kinases that regulate cell cycle check points through initiation of phosphorylation of proteinaceous substrates, using adenosine triphosphate (ATP) as a phosphate donor [1]. In order to maintain homeostasis of normal cells undergoing cellular proliferation, activities of Cdks are tightly controlled. Any abnormality in the normal regulation of the cell cycle process leads to uncontrolled cell growth, which is often regarded as one of the hallmarks of cancer cells [2, 3]. Interruption of a deregulated cell cycle, as a consequence of overactivation of a Cdk, has been accepted as a strategy for treatment of proliferative diseases, such as cancer [4-7].

Identification of several small molecule inhibitors of the Cdk family of kinases and their roles in the treatment of diseased states have been published. Several pharmacophores have been reported as potent Cdk1, Cdk2, Cdk4 and/or Cdk9 inhibitors. Flavopiridol (alvocidib) was one of the first-generation ATP-competitive Cdk inhibitors tested in clinical trials [8]. Olomoucine [9], roscovitine [10], purvalanol [11], paullones [12], butyrolactone [13], oxindoles [14], aminothiazoles [15], benzocarbazoles [16] and pyrimidine [17] derivatives have also been recognized as Cdk inhibitors. Recently, palbociclib has been approved as part of a combination of two drugs that could be used simultaneously for patients with estrogen receptor positive advanced breast cancer [18].

Sometime ago we had found that the natural pigment fascaplysin, isolated from the marine sponge *Fascaplysinopsis* Bergquist sp [19], was a potent inhibitor of Cdk4 [20]. It blocks the cell cycle at the G_0/G_1 phase in both normal and tumor cells [20]. However, it was thought that the planar fascaplysin molecule would be of limited use as an anticancer agent because of its ability to intercalate DNA which causes high toxicity [21]. In our attempts to find non-planar derivatives of fascaplysin, which do not intercalate DNA yet inhibit Cdk4, we had

identified indole and tryptoline derivatives as Cdk4 inhibitors [22-24]. When performing cell cycle analyses with some representative compounds, we had fortuitously found that certain non-planar analogues of fascaplysin also prevent tubulin polymerization [25, 26]. These molecules not only block at the G_0/G_1 phase of the cell cycle due to Cdk4 inhibition, but also at the G_2/M phase due to inhibition of tubulin polymerization. Since they showed high efficacy in mouse tumor models, we had commented that dual inhibitors of Cdk4 and tubulin polymerization, which block cells at two distinctive phases of the cell cycle, should be invaluable in the treatment of cancer [25, 26]. Cdk4 and tubulin polymerization govern the two most important checkpoints (i.e. at the G_0/G_1 and G_2/M phases) in the cell division cycle. The Cdk4 enzyme is considered a target for anticancer therapy because it is deregulated in most, if not all, cancer cells [4-18]. The importance of tubulin polymerization has been exemplified by the regulatory approval of tubulin binding molecules for clinical use, molecules such as the family of compounds known as taxanes and the general use of the vinca alkaloids (one of which is vinblastine) in anticancer therapy [27-30].

Here, we report the construction of a chemical library of 59 quinazolinone derivatives designed on the basis of virtual screening which employed as templates (i.e. 'queries') two molecules which have shown dual inhibitory potential to Cdk4 enzyme and tubulin polymerization [25, 26]. The aim of virtual screening was to identify molecules that may have the potential to bind simultaneously to both Cdk4 and tubulin so that, on the basis of identified structures, chemical libraries could be synthesized to seek molecules that would empirically be capable of inhibiting two crucial targets in the cancer cell division cycle. A Cdk4-cyclin D1 protein kinase assay was initially used to determine whether there were any compounds in a chemical library of quinazolinones, synthesized on the basis of results obtained from virtual screening, which inhibited Cdk4 enzyme. A quinazolinone derivative (i.e. compound **40**; Table 1) was found that inhibits Cdk4 with an IC_{50} value of 0.47 µM. The

IC_{50} values for inhibition of Cdk2-cyclin A2, Cdk1-cyclin B1, Cdk6-cyclin D1 and Cdk9-cyclin T1 were found to be >50 µM. Compound **40** also inhibits tubulin polymerization with an IC_{50} of 0.6 µM. We have named compound **40** as Cink4T (i.e. Compound that inhibits Cdk4 and Tubulin polymerization) in analogy to Cink4, a Cdk4-specific inhibitor with an IC_{50} value of 1.5 µM that we had identified through a high-throughput screen and which was also shown to be efficacious in *in vivo* mouse tumor models [31]. Molecular modelling data tend to support our experimental findings that Cink4T is indeed a dual inhibitor of Cdk4 and tubulin.

At 1x EC_{50} concentration (EC_{50} being the concentration of a drug that gives half-maximal response, in this case inhibition of cancer cell growth), Cink4T blocks growth of pRb (retinoblastoma protein)-positive T47D breast cancer cells at the G_0/G_1 phase of the cell cycle. T47D cells are deficient in the mitotic-spindle checkpoint (MSC)[32], MSC representing the G_2/M cell cycle checkpoint that is affected by drugs that interfere with microtubule (i.e. tubulin) polymerization [33, 34]. Cells deficient in MSC are totally unaffected by such drugs. Hence, Cink4T's inhibitory effects on tubulin polymerization would not be manifested in T47D cells. However, as would be expected of a Cdk4 inhibitor which mediates its cell proliferative function through phosphorylation of pRb [35, 36], Cink4T arrests pRb-positive T47D cells at the early G_0/G_1 phase of the cell cycle and also inhibits Cdk4-specific pRb phosphorylation which is responsible for progression of cells from G_0/G_1, through the restriction point, further into the cell cycle [37-39]. Cink4T also reflects the ability of a true Cdk4 inhibitor by maintaining a block at G_0/G_1 in serum-starved T47D and Calu-1 non-small cell lung carcinoma (NSCLC) cells, both cell types being pRb-positive but MSC-deficient [32, 40]. In stark contrast, we see that Cink4T is unable to arrest MDA-MB-468 breast cancer cells, which are pRb-null but MSC-deficient [41], at G_0/G_1 even at 2x EC_{50} concentration, since the absence of cellular pRb renders a Cdk4 inhibitor (i.e. Cink4T)

non-functional and, thus, completely ineffective. In parallel, in MSC-proficient and pRb-positive A549 NSCLC cells [40], at 1x EC_{50} concentration, Cink4T reveals its Cdk4 and tubulin dual inhibitory potential by trying to block cells at both G_0/G_1 and G_2/M. However, a G_2/M phase block is mainly seen at 2x EC_{50} concentration reflecting Cink4T's ability to inhibit tubulin polymerization.

The results presented here demonstrate, for the very first time, that virtual screening based on already discovered templates [25, 26] can surprisingly lead to the identification of novel molecules that can potently inhibit two crucial phases of the cancer cell division cycle.

2. Results and Discussion

2.1. Virtual screen of quinazolinones that could potentially identify a dual inhibitor of Cdk4 and tubulin polymerization. Shape and electrostatic similarity based virtual screening of ligands can be used as tools in drug discovery, from enriching a huge database of compounds to identification of potential 'hits' [42-45]. It has been claimed that ligand-based virtual screening, used for the identification of dual inhibitors of human immunodeficiency virus-1 (HIV-1) reverse transcriptase and ribonuclease H activities, was the first application of such an approach in the context of HIV-1 research [46].

We have already reported that certain non-planar analogues of fascaplysin can act as dual inhibitors of two important targets of the cancer cell division cycle, the Cdk4 enzyme and tubulin polymerization [25, 26]. Originally, we had only been seeking non-planar molecules, derived from fascaplysin, which would have the ability to inhibit Cdk4 specifically [47]. Quite unintentionally, we had found that some molecules that inhibit Cdk4 also inhibit polymerization of tubulin. These molecules include CA224 [25, 48] and CA199 [49], which is

an analogue of BPT [26]. They do not possess fascaplysin's DNA intercalating property [21] and, hence, are devoid of the toxicity that is associated with fascaplysin.

In an attempt to identify new chemical scaffolds that simultaneously target inhibition of Cdk4 enzyme and tubulin polymerization, shape and electrostatic similarity based virtual screening was performed using OpenEye tools, OMEGA, ROCS and EON. A drug-like subset in the ZINC13 database, having 13,195,609 molecules, was screened with the OpenEye tools. The two non-planar fascaplysin analogues, CA199 [49] and CA224 [25, 48] (depicted in Figure 1), already reported as dual inhibitors of Cdk4 enzyme and tubulin polymerization, were used as templates (i.e. queries). The 'hits' obtained with both the queries were merged and the top 30,000 molecules were picked to provide an enriched library for further molecular docking studies. Protein Preparation Wizard, Ligprep and Glide modules from Maestro-8.5 (Schrodinger LLC) were used to run molecular docking simulation. The enriched-library was subjected to molecular docking against ATP biding site of Cdk4 using X-ray crystal structure of the Cdk4 mimic of Cdk2 (PDB: 1GII)[50] using the XP-protocol in the Glide module. The top 10% 'hits' were then selected for molecular docking against the colchicine ATP-binding pocket of tubulin using the X-ray crystal structure of tau-tubulin kinase in complex with a small molecule inhibitor (PDB: 4BTK) [51]. The top ten 'hits', from molecular docking against both Cdk4 and tubulin, are also shown in Figure 1. They belong to seven different chemical scaffolds which, structurally, are quite different from the fascaplysin analogues reported by us earlier.

2.2. Syntheses of the quinazolinone chemical library. Compounds **5** and **9** (shown in Figure 1), possessing the quinazolinone nucleus, were amongst the top ten 'hits' that showed affinity towards both Cdk4 and tubulin in the virtual screen. In a completely separate drug design program, we had previously identified the quinazolinone scaffold [52] as a mimic of α-

naphthoflavone (ANF), using isosteric replacement strategy. *In vitro,* ANF is known to inhibit potently both CYP1A1 and CYP1B1 isozymes [53] belonging to the drug-metabolizing cytochrome P450 family of enzymes [54, 55]. On the basis of such a screen, we had reported that certain quinazolinone derivatives, based on compounds **5** and **9** (Figure 1), can act as potent and specific inhibitors of CYP1B1 enzyme which is known to have a role in the progression of different tissue-specific cancers [52].

A library of fifty-nine compounds, twenty (**14-20** and **22-34**) which had been reported earlier [52] and thirty-nine new compounds, were synthesized as per the reactions outlined in **Scheme 1**. All the quinazolinone derivatives were formed through condensation, in DMF, of anthranilamide with a corresponding benzaldehyde in the presence of sodium acetate, as base, and iodine as oxidizing agent. Benzaldehydes used for the synthesis of compounds **14**-**34** (Table 1) were synthesized as reported earlier [52]. Benzaldehydes required for the synthesis of compounds **35**-**72** (**Table 1**) were synthesized by refluxing, in acetone, respective 2-chloro-*N*-aryl-aceatamides with corresponding hydroxy benzaldehydes (3-hydroxybenzaldehyde, 4-hydroxybenzaldehyde, vanillin or isovanillin) in the presence of potassium carbonate and potassium iodide. The products thus obtained were purified by washing with an ethyl acetate:petroleum ether (40:60) mixture. Structures of the synthesized compounds (**Table 1**) were confirmed by ^{1}H-NMR, ^{13}C-NMR and MS spectral data (see 4. Experimental section).

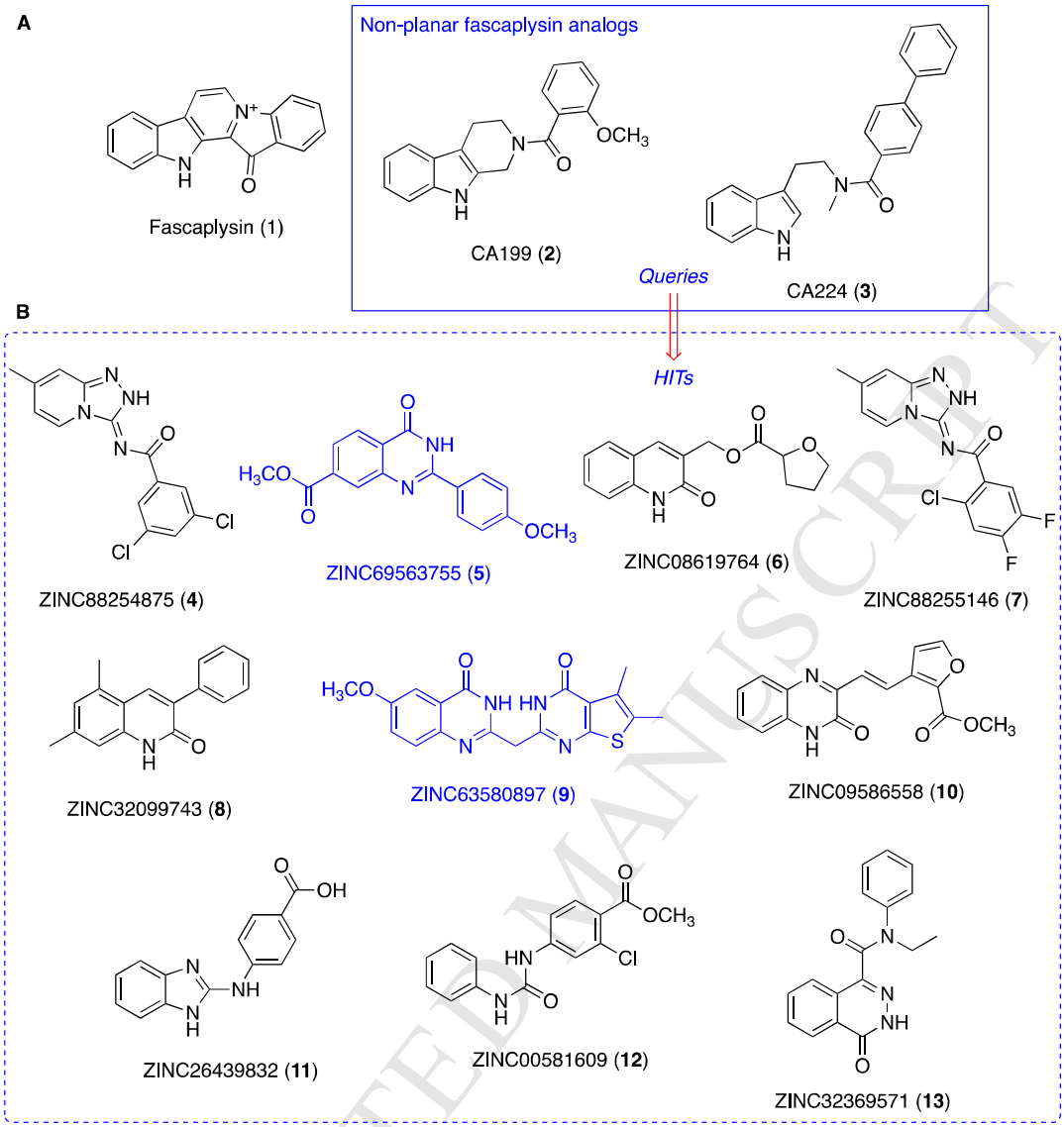

Figure 1. (A) The two 'queries' used for virtual screening. (B) The ten 'hits' obtained from virtual screening.

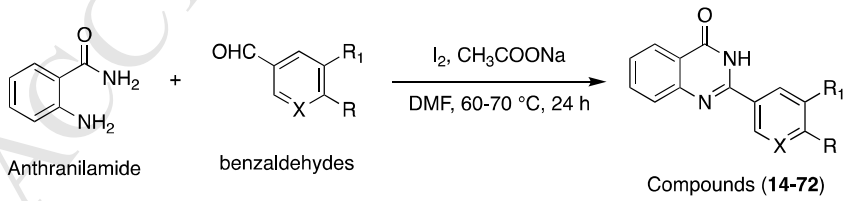

Scheme 1. A general scheme for the syntheses of compounds **14-72**.

Table 1. Structure of quinazolinone derivatives (i.e. compounds **14** to **72**) and their percentage inhibition of Cdk4-cyclin D1 protein kinase, at 10 µM concentration of each compound.

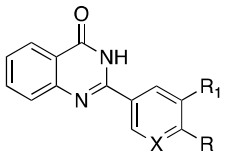

Compounds **14-72**

Code	R	R_1	X	% inhibition of Cdk4-cyclin D1 at 10 µM [a]
14	-H	-H	N	36 ± 1.6
15	$-NO_2$	-H	CH	0 ± 0.3
16	-Br	-H	CH	31 ± 1.5
17	-OH	-H	CH	30 ± 1.2
18	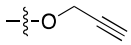	-H	CH	13 ± 0.5
19	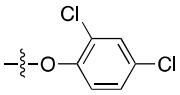	-H	CH	30 ± 1.2
20	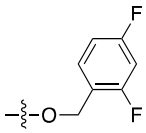	-H	CH	42 ± 1.7
21	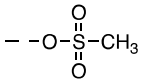	-H	CH	35 ± 1.4
22	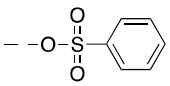	-H	CH	30 ± 1.2
23	-H	-OH	CH	-6 ± 0.5
24	$-OCH_3$	-OH	CH	0 ± 0.3
25	-OH	$-OCH_3$	CH	39 ± 1.2
26	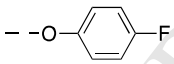	$-OCH_3$	CH	55 ± 1.8
27	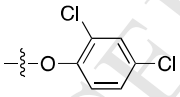	$-OCH_3$	CH	34 ± 1.1
28	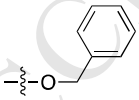	$-OCH_3$	CH	36 ± 1.3
29	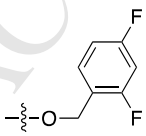	$-OCH_3$	CH	78 ± 2.3
30	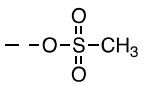	$-OCH_3$	CH	38 ± 1.3
31	$-OCH_3$	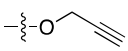	CH	46 ± 1.7
32	$-OCH_3$	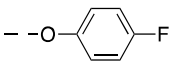	CH	29 ± 1.0
33	$-OCH_3$	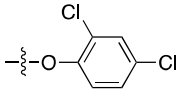	CH	45 ± 1.5

Code	R	R_1	X	% inhibition of Cdk4-cyclin D1 at 10 µM [a]
34	-OCH_3	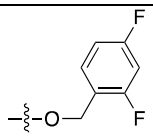	CH	76 ± 2.2
35	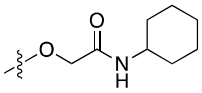	-H	CH	20 ± 0.7
36	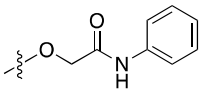	-H	CH	45 ± 1.6
37	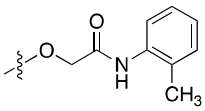	-H	CH	-11±0.7
38	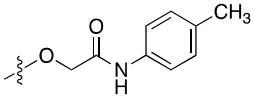	-H	CH	5 ± 0.3
39	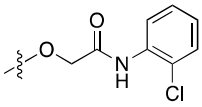	-H	CH	-13 ± 0.7
40 (Cink4T)	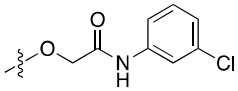	-H	CH	95 ± 3.1
41	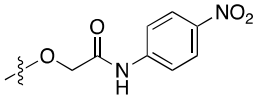	-H	CH	26 ± 0.9
42	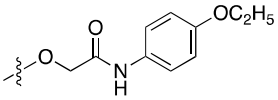	-H	CH	-27 ± 0.8
43	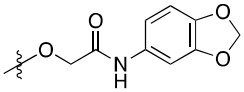	-H	CH	28 ± 1.1
44	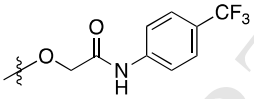	-H	CH	-8 ± 0.6
45	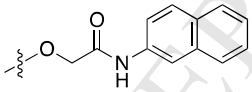	-H	CH	0 ± 0.3
46	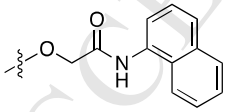	-H	CH	5 ± 0.4
47	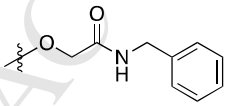	-H	CH	28 ± 0.9
48	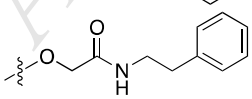	-H	CH	-37 ± 1.1
49	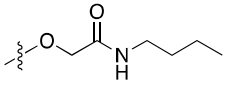	-OCH_3	CH	48 ± 1.4
50	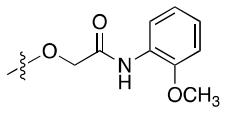	-OCH_3	CH	89 ± 2.8

Code	R	R_1	X	% inhibition of Cdk4-cyclin D1 at 10 µM [a]
51	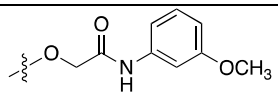	-OCH_3	CH	16 ± 0.7
52	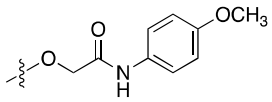	-OCH_3	CH	41 ± 1.4
53	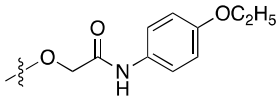	-OCH_3	CH	0 ± 0.4
54	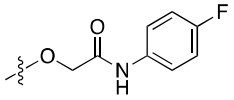	-OCH_3	CH	7 ± 0.4
55	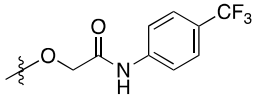	-OCH_3	CH	-3 ± 0.3
56	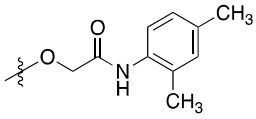	-OCH_3	CH	0 ± 0.3
57	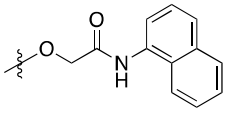	-OCH_3	CH	16 ± 0.5
58	-OCH_3	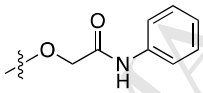	CH	20 ± 0.5
59	-OCH_3	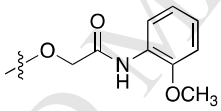	CH	21 ± 0.5
60	-OCH_3	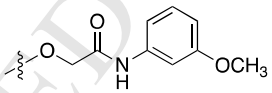	CH	5 ± 0.3
61	-OCH_3	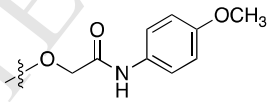	CH	14 ± 0.5
62	-OCH_3	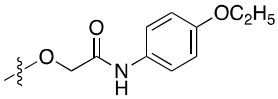	CH	3 ± 0.4
63	-OCH_3	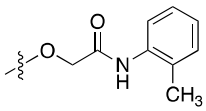	CH	-5 ± 0.4
64	-OCH_3	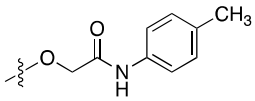	CH	0 ± 0.3
65	-OCH_3	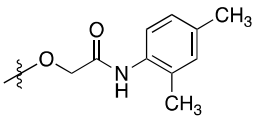	CH	-4 ± 0.3
66	-OCH_3	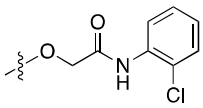	CH	41 ± 1.1
67	-OCH_3	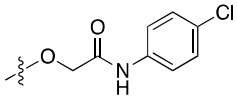	CH	0 ± 0.3

Code	R	R_1	X	% inhibition of Cdk4-cyclin D1 at 10 µM [a]
68	-OCH_3	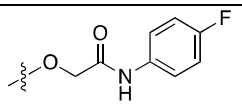	CH	-12 ± 0.5
69	-OCH_3	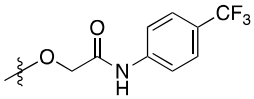	CH	-3 ± 0.4
70	-OCH_3	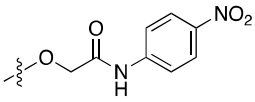	CH	1 ± 0.3
71	-OCH_3	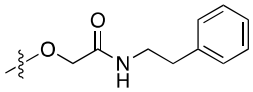	CH	-10 ± 0.5
72	-OCH_3	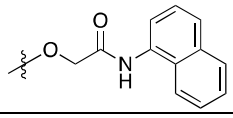	CH	39 ± 0.8

[a] Percentage inhibition represent mean and standard deviations from three independent experiments.

2.3. Screening of the quinazolinone chemical library in the Cdk assays. The library of fifty-nine quinazolinones, at 10 µM concentration, was at first screened in the Cdk4-cyclin D1 kinase assay using a C-terminal fragment of pRb (i.e. RBCTF) [56] as substrate, as suggested by the supplier of the assay (ProQinase, Germany). Out of the fifty-nine quinazolinones synthesized, fifty-six compounds were derived from hydroxy benzaldehydes (3-hydroxybenzaldehyde, 4-hydroxybenzaldehyde, vanillin or isovanillin) and their derivatives. The aryl group of these benzaldehydes constitutes the pendent phenyl ring at 2nd position of quinazolinones (compounds **17** to **72**; **Table 1**). Hydroxyl groups of these four benzaldehydes provided an opportunity to extend the sidechain of pendent phenyl ring at its *meta*- and *para*-positions. 4-hydroxy derivative (compound **17**) displayed 30% inhibition at 10 µM concentration. Substitution of 2,4-diflurobenzyl-oxy group (compound **20**) marginally improved its activity to 42%. An additional methoxy functional group *ortho*- to 4th-position did not show any significant improvement in activity with reference to compounds bearing 2,4-dichlorophenyl-oxy (compounds **19, 27**) and methyl sulphonyl (compounds **21, 30**) substitutions. Whereas, compounds bearing 2,4-diflurobenzyl-oxy substitution (compounds **20, 29**), have significantly improved activity, that is,78% inhibition at 10 µM concentration.

Swapping the position of these two functional groups provided compound **34** with similar activity (76% inhibition at 10 µM). Introduction of -CO-NH- between -OCH2- and -R provided an oxy-acetanilide side chain (compounds **35** to **72**; Table 1). Compound **36** carrying oxy-acetanilide with unsubstituted phenyl ring exhibited 45% inhibition at 10 µM concentration. Substitution at *ortho*- (compounds **37**, **39**) and *para*- (compounds **38**, **41**, **42**, **44**) positions of phenyl ring of oxy-acetanilide group (compounds **37**, **39**, **40**), ring fusion (compounds **43**, **45, 46**), replacing phenyl with Ar-alkyl (compounds **47, 48**) did not provide better activity in comparison with compound **36**. While, chloro- substitution at *meta*- position of phenyl ring of oxy-acetanilide group, provided the best compound **40**, in this series, with 95% inhibition at 10 µM concentration. In order to comment on the effects of additional methoxy group *ortho*- to 4-oxyacetanilide substitution would require further library enumeration as current set of compounds **49**-**57** do not share similarity at 4th position when comparing with compounds **35**-**48**. But a compound having *ortho*-methoxy substitution on phenyl ring of oxy-acetanilide (**50**) has showed 89% inhibition at 10 µM concentration. Swapping the position of methoxy and oxy-acetanilide substitutions (**58**-**72**) decreased the activity. In summary, (i) diflurobenzyl-oxy substitution at 3rd or 4th position of pendent phenyl ring with an ortho-methoxy functional group, (ii) oxy-acetanilide with 3-chloro substitution in its phenyl ring at 4th position of pendent phenyl ring and (iii) oxy-acetanilide with 2-methoxy substitution on its phenyl ring at 4th position of pendent phenyl ring along with an ortho-methoxy functional group are favorable for Cdk4 inhibitory activity.

Four compounds **29**, **34**, Cink4T (**40**) and **50** were identified as having >75% inhibition at 10 µM concentration (Table 1). These compounds were further screened for percentage inhibition, at 10 µM concentration, in the Cdk2-cyclin A, Cdk1-cyclin B1, Cdk9-cyclin T1, and Cdk6-cyclin D1 kinase assays (Table 2), using a C-terminal fragment of pRb (RBCTF) or RBER CHKtide as substrates, depending on the Cdk, as suggested by the supplier (ProQinase,

Germany). RBER CHKtide consists of an N-terminal GST tag linked to amino acids S773-K928 of pRb (National Center for Biotechnology Information, NCBI Accession # NP_000312) which is followed by 11 Arg residues and the 23-amino acid peptide sequence, KKKVSRSGLY RSPSMPENLN RPR (CHKtide).

After determination of percentage inhibition of the four different Cdk enzymes (Table 2), IC_{50} values, with respect to inhibition of the four kinases, were ascertained for the four compounds **29**, **34**, Cink4T and **50** (Table 2). All four compounds were found to be selective inhibitors of Cdk4-cyclin D1 enzyme with low micromolar Cdk4 IC_{50} values, ranging from 0.47 µM to 3.8 µM (Table 2). Amongst the four compounds, Cink4T was the most potent with an IC_{50} value of 0.47 µM which was similar to that observed earlier with fascaplysin (0.41 ± 0.04 µM)[20] and much lower than the IC_{50} values of fascaplysin's two published non-planar analogues BPT (10 ± 1.2 µM) [26] and CA224 (6.2 ± 0.9 µM) [25], which had also been found to be efficacious in mouse tumor models. Cink4T (i.e. compound **40**) and compound **50** were also tested for inhibition of CYP1A1, CYP1A2 and CYP1B1 enzymes. They had IC_{50} values of >5 µM for each of the three enzymes in microsomal enzyme assays [52], microsomal enzymes being endoplasmic reticular membrane-bound CYP enzymes which are isolated from recombinant insect or yeast cells. Compounds **29** and **34** have never been reported before. They also have IC_{50} values of >5 µM in the three CYP1 microsomal assays (unpublished observations).

Table 2. IC_{50} values of the four most potent Cdk4 inhibitors, as identified in Table 1, in Cdk4-cyclin D1, Cdk2-cyclin A2, Cdk1-cyclin B1, Cdk9-cyclin T1 and Cdk6-cyclin D1 kinase assays. Results demonstrate Cdk4-specificity of the four compounds vis-à-vis the three kinases Cdk2-cyclin A2, Cdk1-cyclin B1 and Cdk9-cyclin T1. Pablociclib, the US Food and Drug Administration (FDA)-approved Cdk4 inhibitor [57], was used as a control.

Code	%Inhibition Cdk4/cycD1, at 10 µM (IC_{50}, µM) [a]	% Inhibition Cdk2/cycA2, at 10 µM (IC_{50}, µM) [a]	% Inhibition Cdk1/cycB1, at 10 µM (IC_{50}, µM) [a]	% Inhibition Cdk9/cycT1, at 10 µM (IC_{50}, µM) [a]	%Inhibition Cdk6/cycD1, at 10 µM (IC_{50}, µM) [a]
Cink4T (40)	95 ± 3.1 (0.47 ± 0.06)	-18 ± 0.8 (>100)	8 ± 0.3 (>50)	-15 ± 0.7 (>100)	-22 ± 1.1 (>100)
29	78 ± 2.3 (3.5 ± 0.2)	-8 ± 0.4 (>100)	13 ± 0.6 (>50)	-5 ± 0.2 (>100)	-15 ± 08 (>100)
34	76 ± 2.2 (3.8 ± 0.3)	-5 ± 0.2 (>100)	10 ± 0.4 (>50)	8 ± 0.3 (>50)	-18 ± 0.9 (>100)
50	89 ± 2.8 (1.5 ± 0.1)	14 ± 0.7 (>50)	14 ± 0.6 (>50)	-22 ± 0.8 (>100)	-14 ± 0.7 (>100)
Pablociclib (obtained values)	95 ± 2.5 (0.013 ± 0.002)	42 ± 1.7 (>10 µM)	5 ± 0.4 (>100 µM)	-4 ± 0.5 (>100 µM)	-97 ± 0.7 (0.018 ± 0.002)
Pablociclib (published values)[57]	(IC_{50}: 0.011)	(IC_{50}: >10 µM)	(IC_{50}: >10 µM)	(IC_{50}: ND)	(IC_{50}: 0.016)

[a] Percentage inhibition of the Cdk4, Cdk2, Cdk1, and Cdk9 enzymes and the IC_{50} values for inhibition of enzyme activities represent mean and standard deviations (where applicable) from three independent experiments. 'ND' denotes not determined.

2.4. Comparison of the ability of the four Cdk4 inhibitors, compounds 29, 34, Cink4T and 50, to inhibit tubulin polymerization in vitro, at 5 µM concentration. Cink4T had been identified in the chemical library that was designed on the basis of a virtual screen which aimed to find dual inhibitors of Cdk4 and tubulin. The templates ('queries') that were used for this virtual screen were two known dual inhibitors of Cdk4 and tubulin polymerization [25, 49]. Hence, we investigated next the action of Cink4T on tubulin polymerization *in vitro*.

The original procedures [58, 59] for determination of tubulin polymerization depend on light being scattered by microtubules in a way that light scattering is proportional to increase in microtubule polymer concentration. The curve, that results from observations of light scattering of tubulin polymerization over a period of time, is representative of the three phases of microtubule polymerization: (i) nucleation, (ii) growth and (iii) steady state equilibrium.

The fluorescence-based tubulin polymerization assay, used in our studies, has been adapted from a protocol described earlier [60]. It is a quick one-step procedure for determining the effects of drugs on tubulin polymerization and it compares well with the absorbance-based

assay (Tubulin polymerization assay kit; Cytoskeleton Inc; Cat # BK011P; https://www.cytoskeleton.com/bk011p). Tubulin polymerization is tracked by fluorescence enhancement due to the incorporation of a fluorescent reporter into microtubules that occurs with the progression of polymerization. Porcine neuronal tubulin, used for the experiments, was of the highest available purity (>99% pure, Cytoskeleton, Cat. # T240).

Representative polymerization curves of paclitaxel (an enhancer of tubulin polymerization), compounds **29**, **34**, **50** and Cink4T are shown in Figure 2. Compounds that interact with tubulin alter one or more of the characteristic phases of polymerization. For example, at 3 µM concentration paclitaxel eliminates the nucleation phase and enhances the V_{max} of the growth phase. In contrast, vinblastine, a microtubule destabilizing drug (i.e. a tubulin polymerization inhibitor belonging to the family of vinca alkaloids), causes a drastic decrease in V_{max} and reduction in final polymer mass (Tubulin polymerization assay kit; Cytoskeleton Inc; Cat # BK011P; https://www.cytoskeleton.com/bk011p) [61]. Our results indicate that, at 5 µM concentration, Cink4T interacts with tubulin more strongly than compounds **29**, **34** and **50**, suggesting that it is the most potent tubulin polymerization inhibitor identified in our studies. The Cink4T curve resembles the one obtained with 3 µM vinblastine same fluorescence-based assay. The 'Control' curve, with no drug, relates to the reaction when tubulin is incubated alone (i.e. in the absence of any drug).

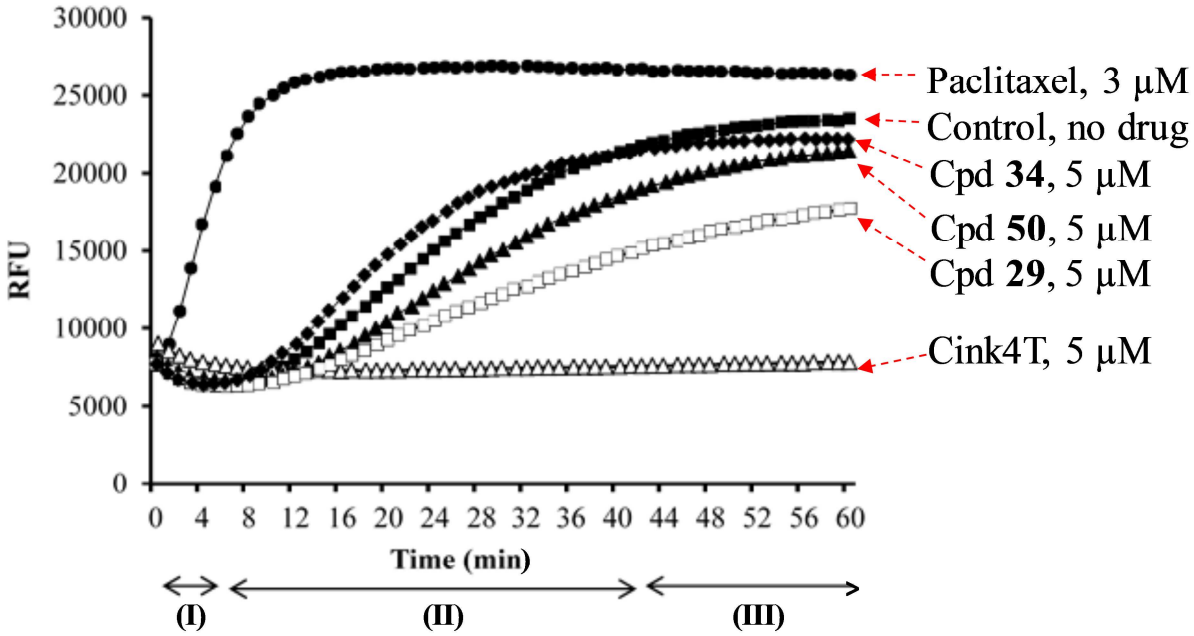

Figure 2. Tubulin polymerization using the fluorescence-based tubulin polymerization assay (BK011P; Cytoskeleton Inc). Tubulin was incubated (a) alone (Control), (b) with paclitaxel, and (c) with compounds **29**, **34**, 5**0** and Cink4T. Each curve represents the average of results performed four times. Polymerization was measured at excitation wavelength of 360 nm and emission at 420 nm. The three phases of tubulin polymerization are marked for the Control (no drug) polymerization curve; I: nucleation, II: growth, III: steady state equilibrium. 'Cpd' signifies 'compound'.

2.5. The ability of the Cdk4 inhibitor, Cink4T, to inhibit tubulin polymerization at different concentrations. Cink4T was then tested over a range of concentrations for its ability to inhibit tubulin polymerization in the same fluorescence-based assay. Again, paclitaxel was used in the assay as a known enhancer of tubulin polymerization. Figure 3 shows the dose response of Cink4T in the process of polymerization of tubulin.

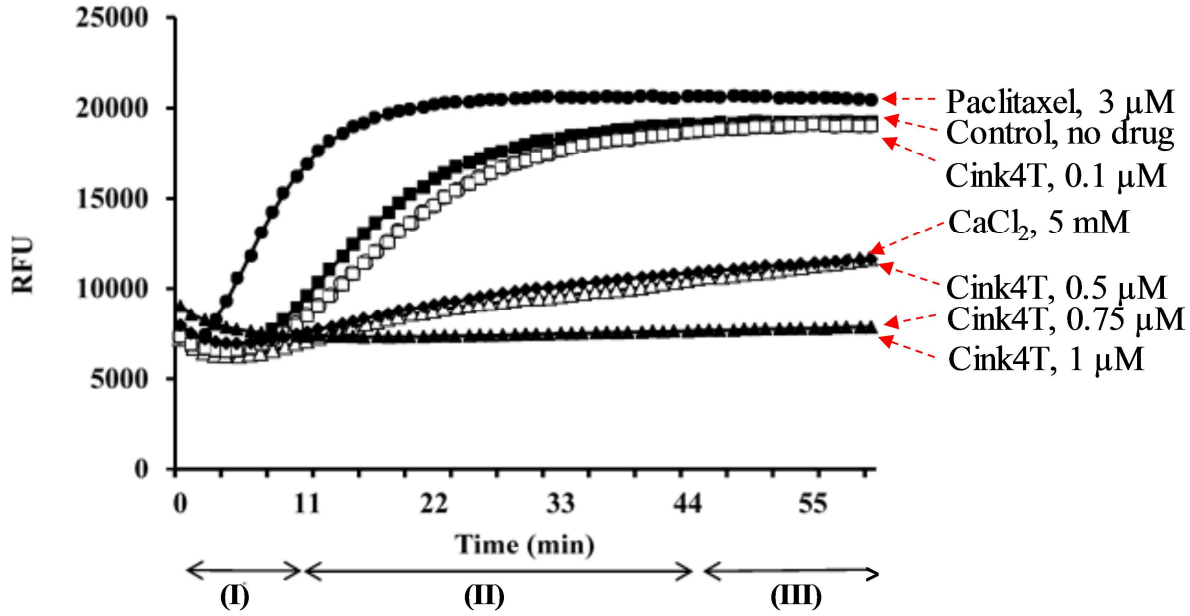

Figure 3. Dose response of Cink4T to inhibition of tubulin polymerization. Tubulin polymerization was determined using the fluorescence-based tubulin polymerization assay (BK011P; Cytoskeleton Inc). Tubulin was incubated alone (Control, i.e. 'no drug'), and with (a) the polymerization enhancer paclitaxel, (b) the depolymerization agent $CaCl_2$, and (c) Cink4T at four different concentrations (0.1, 0.5, 0.75, 1 µM). Each curve represents the average of results performed four times. Polymerization was measured at excitation wavelength of 360 nm and emission at 420 nm. The three Phases of tubulin polymerization are marked for the Control (no drug) polymerization curve; I: nucleation, II: growth, III: steady state equilibrium. The IC_{50} for inhibition of tubulin polymerization by Cink4T was calculated to be 0.6 µM, vinblastine's IC_{50} being also 0.6 µM (Tubulin polymerization assay kit; Cytoskeleton Inc; Cat # BK011P).

2.6. Molecular modeling studies with Cink4T and Cdk4 or tubulin. Cink4T exhibited ~212-fold selectivity towards ATP binding pocket of Cdk4 in comparison with Cdk2. Molecular docking simulation was carried out with AutoDock-4.2. High-scoring conformation from the largest cluster was considered for the analysis of the molecular interaction. Cink4T was found to interact with ATP-binding pocket of Cdk4 in an inverted bend conformation in comparison with a linear conformation in the ATP-binding pocket of Cdk2 (Figure 4). Quinazolinone N3 amino hydrogen and C4 carbonyl oxygen establishes two H-bonds with backbone carbonyl oxygen and amino hydrogen of Val96. These interactions

keep the quinazolinone nucleus in the pocket with the sidechain oxy-acetamido group extending to the entrance of the pocket. Sidechain amino hydrogen of the Arg101's planar guanidine group establishes an additional H-bonding interaction with sidechain carbonyl oxygen of Cink4T, thus forcing the molecule to adopt a *cis*-conformation for maximizing the hydrophobic interaction of Cink4T with Ile12, Val20, Ala33, Lys35, His95, Asp97, Gln98, Asp99, Glu144, Leu147 and Asp158. Interaction of Cink4T with Cdk2 in comparison with Cdk4 revealed that it misses two crucial interactions with Lys88 (Arg101, Cdk4) and Gln131(Glu141, Cdk4) and that may be the reason for its selectivity towards Cdk4. Figure 5 displays 2D-interaction plot for Cink4T with Cdk4 and Cdk2.

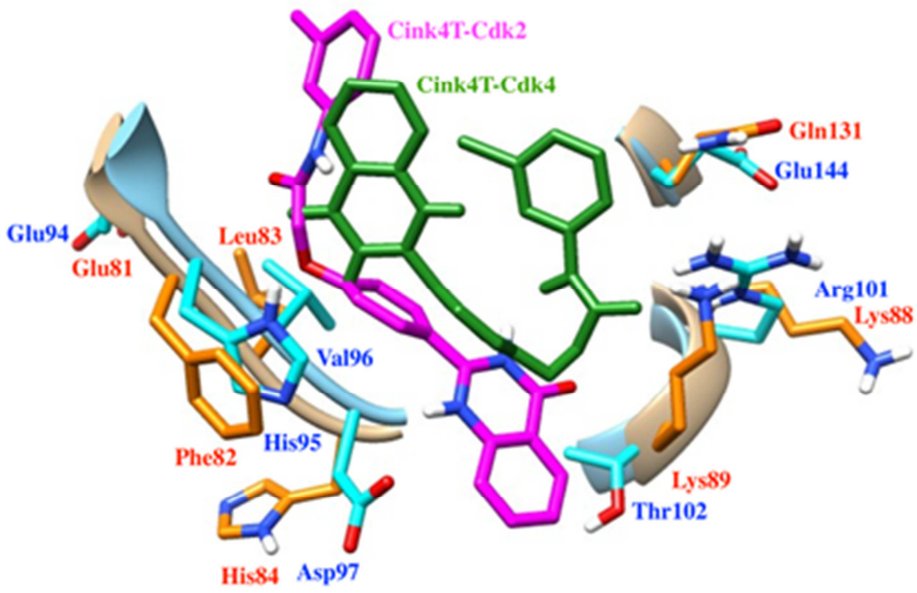

Figure 4. Interactions of Cink4T with Cdk2 and Cdk4. Cdk2 active site residues in orange ribbon with sidechains represented by orange tubes and heteroatoms colored by atom type; Cink4T in Cdk2's pocket is represented by magenta tubes and heteroatoms are colored by atom type. Cdk4 active site residues are in cyan ribbon with sidechains represented by cyan tubes and heteroatoms colored by atom type; Cink4T in the Cdk4 pocket is represented by forest green tubes and heteroatoms are colored by atom type.

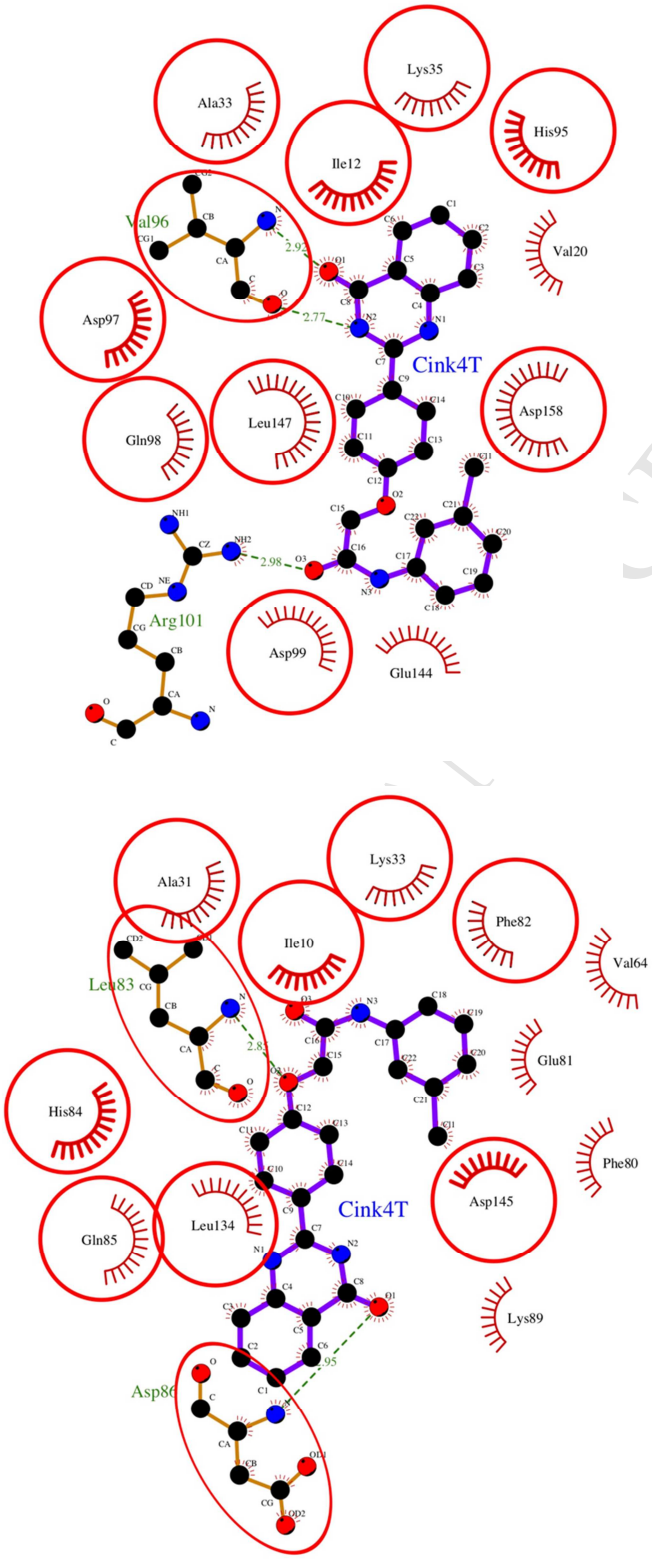

Figure 5. 2D-plot of Cink4T with Cdk4 (top) and Cdk2 (bottom). Hydrogen bonds are represented as green dotted lines; hydrophobic interactions are shown by red lines and equivalent residues are shown as red circles.

Cink4T's interaction with tubulin has been studied at the binding pocket in the interface of tubulin-α/β subunit. No H-bonding interaction was found. Instead, Cink4T exhibited hydrophobic interactions with the following residues in the β-subunit: Val238, Cys241, Leu242, Leu248, Ala250, Lys254, Leu255, Asn258, Ala316, Lys352, Thr353 and Ala354. The following four residues from the α-subunit, Asn101, Ser178, Thr179 and Ala180, displayed hydrophobic interactions with the sidechain oxy-acetanilide portion of Cink4T. Figures 6 shows the interactions of Cink4T with active site residues of tubulin.

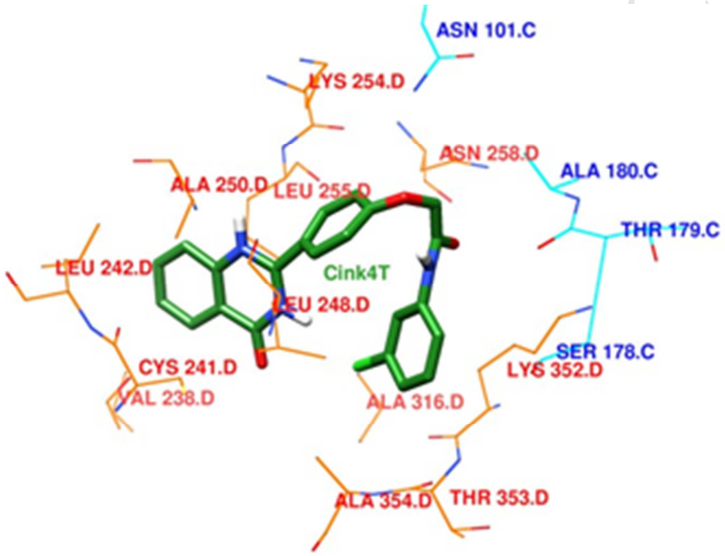

Figure 6. Interaction of Cink4T with tubulin. Sidechains of residues from β-subunit lining the pocket are in orange wires with heteroatoms colored by atom type; sidechains of residues from α-subunit lining the pocket are in cyan wires with heteroatoms colored by atom type. Cink4T is represented by forest green tubes with heteroatoms colored by atom type.

2.7. Cancer cell growth inhibition. EC_{50} values for inhibition of cell growth by the four compounds **29**, **34**, Cink4T (**40**) and **50** were then determined. The four cancer cell lines: A549 (mitotic spindle checkpoint-(MSC)-proficient, pRb-positive, p53-positive), Calu-1 (MSC-deficient, pRb-positive, p53-null), MDA-MB-468 (MSC-deficient, pRb-null, p53 mutant), and T47D (MSC-deficient, pRb-positive, p53 mutant) were chosen for these studies. The EC_{50} values (an EC_{50} value being the concentration of a drug that gives half-maximal response, in this case specifically inhibition of growth of cancer cells) obtained are presented

in Table 3. Compounds **29**, **34** and **50** displayed cell proliferation inhibitory activity ≤ 10 µM concentration in the three pRb-positive cell lines studied (i.e. T47D, Calu-1 and A549), pRb being the sole mediator of active Cdk4-triggerred cell proliferation [35, 36], while Cink4T (**40**) inhibited cell proliferation at sub-micromolar concentrations in the pRb-positive cell lines.

Table 3. Growth inhibition of four cancer cell lines treated with the four Cdk4 inhibitors which were identified in the quinazolinone chemical library, designed on the basis of ligand-based virtual screening.

Compound	A549, EC_{50} (µM) [a]	Calu-1, EC_{50} (µM) [a]	MDA-MB-468, EC_{50} (µM) [a]	T47D, EC_{50} (µM) [a]
Cink4T (40)	0.8 ± 0.05	0.9 ± 0.05	10.85 ± 0.6	0.75 ± 0.06
29	7 ± 0.6	9 ± 0.7	>50	8 ± 0.7
34	7.5 ± 0.7	9.8 ± 0.6	>50	8.2 ± 0.65
50	3 ± 0.2	6 ± 0.4	>50	4 ± 0.3
Palbociclib	0.4 ± 0.02	33 ± 2.2	1.9 ± 0.2	0.35 ± 0.03

[a] Percentage inhibition represent mean and standard deviations from three independent experiments.

2.8. Cink4T blocks growth of asynchronous MSC-deficient, pRb-positive T47D breast cancer cells at G_0/G_1. Upon treatment with 1x EC_{50} (0.75 µM) concentration of Cink4T for 18 h, T47D cells were found to be blocked at G_0/G_1 (compare Figures 7A and 7B). T47D cells are not arrested at G_2/M by Cink4T because they are mitotic spindle checkpoint (MSC)-deficient[32]; MSC-proficiency is required for a G_2/M block mediated by a compound that has a role in tubulin polymerization [25, 26, 33, 62]. The block at G_0/G_1 phase observed in cells treated with Cink4T would suggest inhibition of cellular Cdk4 which acts at G_0/G_1. Further cell cycle analysis showed that treatment of cells with 2x EC_{50} (1.5 µM) concentration of Cink4T leads to induction of apoptosis, which is displayed by the sub-G1 peak in Figure

7C. It has been observed that a compound which induces block of cancer cells at G_0/G_1 often induces apoptosis [31, 63, 64].

The phosphorylation status of Cdk4-specific serine residues, Ser780, Ser795 and Ser807/811 in pRb (i.e. serine residues in pRb that are specifically phosphorylated by Cdk4-cyclin D1) [38, 39, 65] was assessed in untreated T47D cells together with cells treated with Cink4T, at 1x EC_{50} (0.75 µM) and 2x EC_{50} (1.5 µM) concentrations, via Western blotting (Figures 7D to 7G). Phosphorylation of these residues modify the conformation of pRb to allow progression of cells in the cell cycle [39]. The Western blots (Figures 7E and 7F) demonstrate that Cink4T, at both 1x EC_{50} and 2x EC_{50} concentrations, inhibits the phosphorylation of pRb at the Ser780 and Ser795 residues, thus suggesting Cdk4-specific activity of Cink4T. Although Cink4T fails to prevent phosphorylation of pRb at the Ser807/11 residues at 1x EC_{50} concentration, it does so at the higher 2x EC_{50} concentration (Figure 7G). Lower levels of pRb at 2x EC_{50} concentration of Cink4T (Figure 7D) may suggest that cells were apoptotic which was actually seen from the sub-G_1 peak in the cell cycle analysis (Figure 7C).

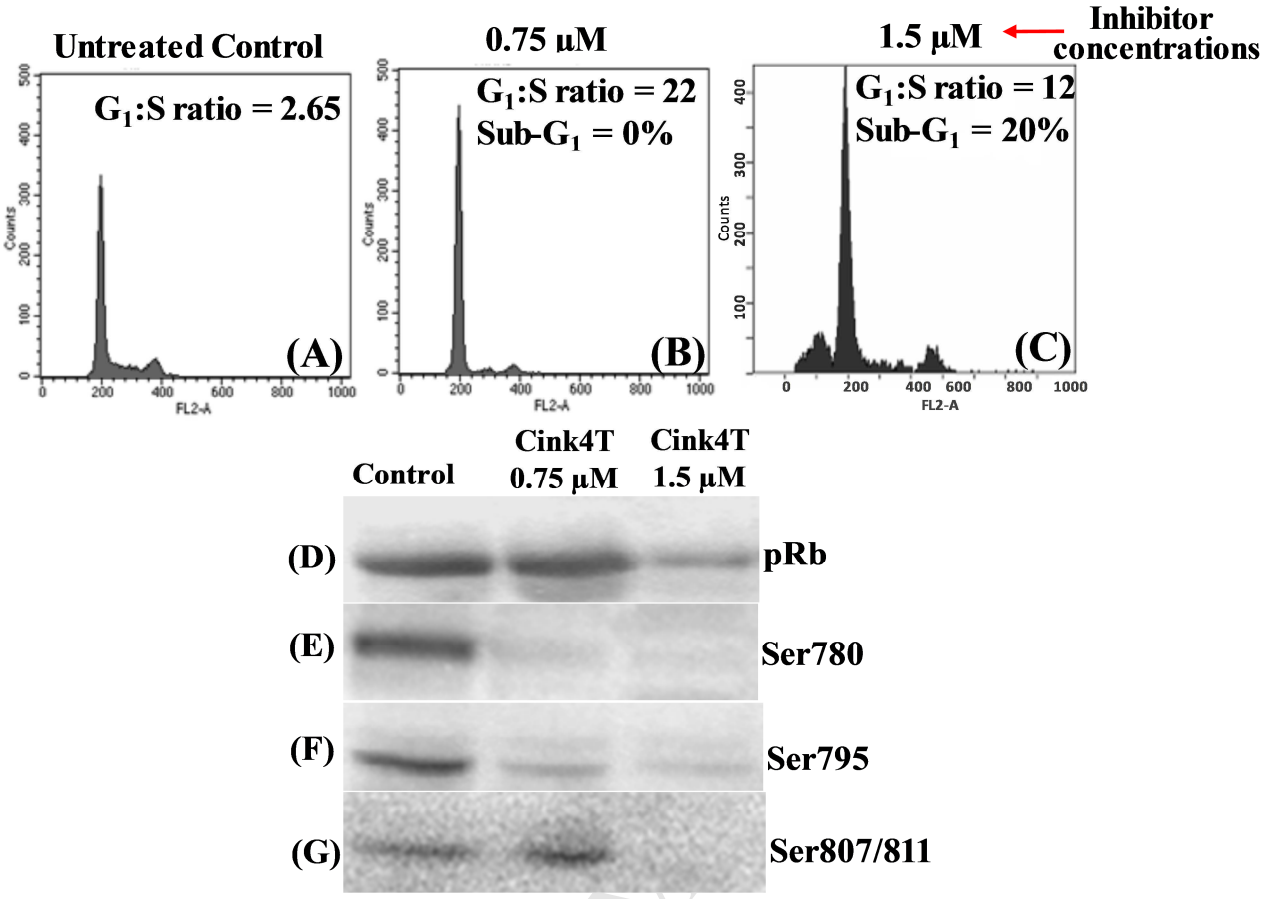

Figure 7. (A) to (C): Cell cycle analyses of T47D (MSC-deficient, pRb^{+}) cells which are treated with 1x EC_{50} (0.75 µM) and 2x EC_{50} (1.5 µM) concentrations of Cink4T for 18 h. The ratio between G_0/G_1 and S phases of the cell cycle (i.e. G_1:S ratio), increases dramatically upon treatment with Cink4T which is indicative of a block at G_0/G_1. The sub-G_1 peak indicates apoptosis. (D) to (G): Western blot analysis of proteins from untreated cells (i.e. Control) and T47D cells treated for 18 h with 1x EC_{50} (0.75 µM)) and 2x EC_{50} (1.5 µM) concentrations of Cink4T, using phospho-specific antibodies (Ser780, New England Biolabs, Cat # 9307; Ser795, New England Biolabs, Cat # 9301; Ser807/811, New England Biolabs, Cat # 9308) and an antibody to pRb (New England Biolabs, Cat # 9309). An appropriate HRP-conjugated secondary antibody was used to illuminate the different forms of pRb (phosphorylated and unphosphorylated).

2.9. Cink4T maintains block of cell growth at G_0/G_1, induced by serum starvation, of MSC-deficient, pRb-positive T47D breast cancer and Calu-1 non-small cell lung carcinoma (NSCLC) cells. Cdk4 is the first cyclin dependent kinase that is activated upon entry of cells in the cell division cycle, that is, at the G_0/G_1 phase transition. The activation of Cdk4 by cyclin D1 initiates the phosphorylation of pRb that ultimately causes its dissociation

from the E2F family of transcription factors leading to a cascade of events that result in the entry of cells into the S phase [66]. The transition from G_0 to G_1 phase of the cell cycle is dependent on serum growth factors present in the cell culture medium. When cells are starved of serum, they undergo arrest at the G_0/G_1 boundary but when fresh serum is added to these cells, the arrested cells re-enter the cell cycle. We hypothesized that if Cink4T truly inhibits Cdk4-cyclin D1 enzyme in cells, serum-starved cells would not re-enter the cell cycle if they were released in the presence of Cink4T. In order to block the cells at early G_1 phase, T47D and Calu-1 cells were serum starved by incubating in medium containing 0.1% FBS (fetal bovine serum) for 24 h. They were then released in complete growth medium supplemented with 10% FBS in the presence or absence of test compound for a further 18 h.

Flow cytometric analysis of T47D and Calu-1 cells show that, upon serum starvation, ~85% and ~88% percentage of cells reside at the G_0/G_1 phase of the cell cycle (Figures 8A and 7E). Serum-starved cells, when released just in the presence of fresh medium, entered the cell cycle normally with 60% and 69% cells at G_0/G_1 and percentage increase in S phase of around 11% (Figures 8B and 8F). Serum-starved cells, synchronized at G_0/G_1, released in the presence of 1x EC_{50} concentration of Cink4T is prevented from fully re-entering the cell cycle (Figures 8C and 8G). The G_0/G_1 block is somewhat maintained with 77% and 75% cells being found in the G_0/G_1 phase. When the serum starved cells were released in the presence of 2x EC_{50} concentration of Cink4T (Figures 8D and 8H), G_0/G_1 arrest was fully maintained in Calu-1 cells but apoptosis was induced in T47D cells. 18.6% of T47D cells were detected in the sub-G_1 peak which indicates apoptotic cells (Figure 8D) suggesting that at the higher concentration of Cink4T induction of apoptosis is seen only in T47D cells, which carry a *p53* mutant allele, at the G_0/G_1 phase of the cell cycle. Calu-1 cells, which completely lack the *p53* gene (i.e. are p53-null), are resistant to apoptosis [67]. Overall, cell cycle analyses show that

Cink4T displays the typical characteristic of a true Cdk4 inhibitor by maintaining G_0/G_1 arrest in the cell cycle when cells are released in fresh medium after serum starvation [25, 26].

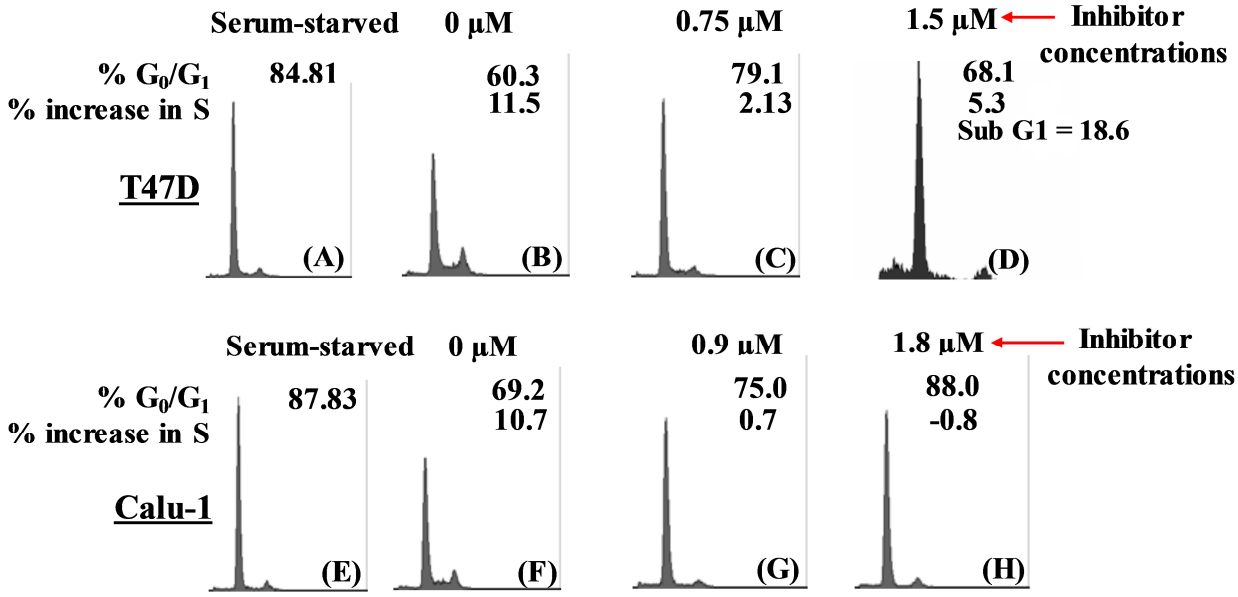

Figure 8. Cell cycle analyses of the response of T47D and Calu-1 cells, synchronized through serum starvation, to treatment with Cink4T. (A), (E): synchronized, serum-starved T47D and Calu-1 cells; (B), (F): serum-starved cells released in fresh medium for 18 h; (C), (G): serum-starved cells released into fresh medium in the presence of 1x EC_{50} concentration of Cink4T for 18 h; and (D), (H): serum-starved cells released into fresh medium in the presence of 2x EC_{50} concentration of Cink4T for 18 h.

2.10. Cink4T is unable to block growth of asynchronous MSC-deficient but pRb-null MDA-MB-468 breast cancer cells at G_0/G_1. Inhibition of Cdk4-mediated block of cell growth at G_0/G_1 depends on the presence of pRb within the cells [35, 36], while cells which are mitotic spindle checkpoint (MSC)-deficient are unaffected by tubulin polymerization inhibitors[33, 62]. Hence, it would be expected that MDA-MB468 cells which lack the retinoblastoma gene, *pRb*, and are also MSC-deficient [41] are mainly unaffected by increasing concentrations of Cink4T (compare Figure 9A with 9B and 9C). Indeed, MDA-MB468 cells do not undergo cell cycle block at G_0/G_1 or undergo apoptosis as is indicated by the ratio of the peaks observed at the G_0/G_1 and S phases (G_1:S ratio), and the sub-G_1 peak,

upon treatment of cells with 1x EC_{50} (10.85 µM) and 2x EC_{50} (22 µM) concentrations of Cink4T for 18 h (Figures 9B and 9C).

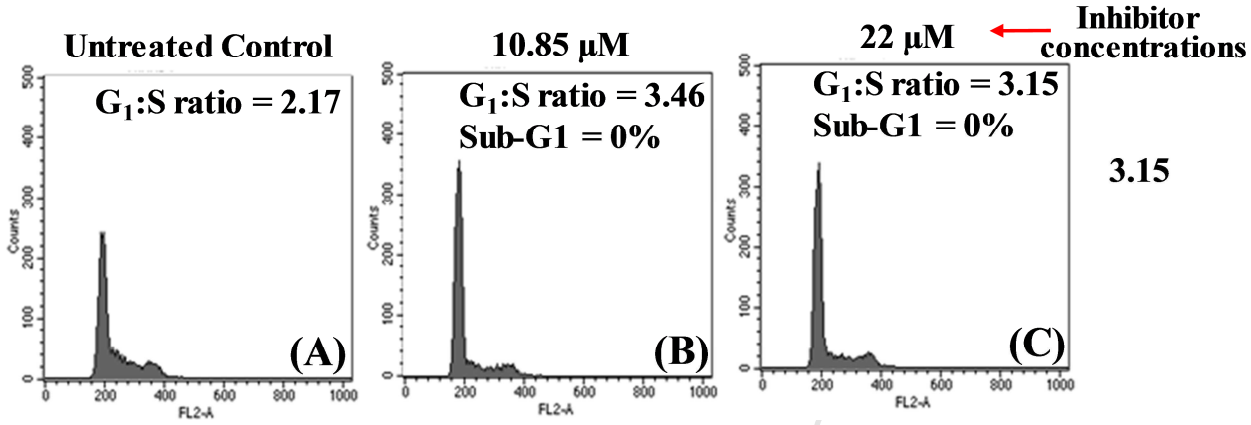

Figure 9. (A) to (C): Cell cycle analyses of MDA-MB-468 (MSC-deficient, pRb-null) cells which are treated with 1x EC_{50} (10.85 µM; B) and 2x EC_{50} (22 µM; C) concentrations of Cink4T for 18 h. The ratio between G_0/G_1 and S phases of the cell cycle (G_1:S ratio), with increasing concentrations of Cink4T, are shown within each cell cycle analysis, (A) to (C). The sub-G_1 peak, which is 'zero', would indicate that MDA-MB-468 cells do not undergo any apoptosis upon treatment with Cink4T.

2.11. Cink4T blocks growth of asynchronous MSC-proficient, pRb-positive A549 non-small cell lung carcinoma (NSCLC) cells at G_2/M. In MSC-proficient A549 cells which also carry a functional *pRb* gene [40], cells undergo an increase in the G_1/S ratio (from 2.7 to 6.5) together with an increase in the percentage of cells at G_2/M (from 18% to 28%) when treated, for 18 h, with 1x EC_{50} (0.8 µM) concentration of Cink4T (compare Figures 10A and 10B). However, a G_2/M block becomes obvious, with percentage of cells at G_2/M being 70%, when A549 cells are treated with 2x EC_{50} (1.6 µM) concentration of Cink4T (Figure 10C). The results show the accumulation of A549 cells, in which the mitotic spindle checkpoint is intact, predominantly at mitosis (i.e. G_2/M) only when cells are treated with the higher concentration of Cink4T. They also indicate that Cink4T, designed on the basis of a virtual screen, not only arrests cells at the early G_0/G_1 phase of the cell cycle but also at mitosis (i.e. G_2/M phase of the cell cycle).

Upregulation of expression of cyclin B1 is considered as a marker for G_2/M arrest of the cell cycle that is induced by tubulin inhibitors[68-70]. Hence, we assessed the status of cyclin B1, together with its cognate protein Cdk1, in A549 cells after treatment with Cink4T (Figures 10D and 10F), via Western blotting. The results show that cells blocked at G_2/M, when treated with 2x EC_{50} (1.6 µM) concentration of Cink4T, do have remarkable increase in the levels of cyclin B1 (Figure 10D) but, as would be expected, Cdk1 levels remain unchanged (Figure 10F). Our cell cycle results and Western blot data strongly indicate that Cink4T very likely affects a target at the G_2/M phase of the cell cycle. The target is very likely to be tubulin.

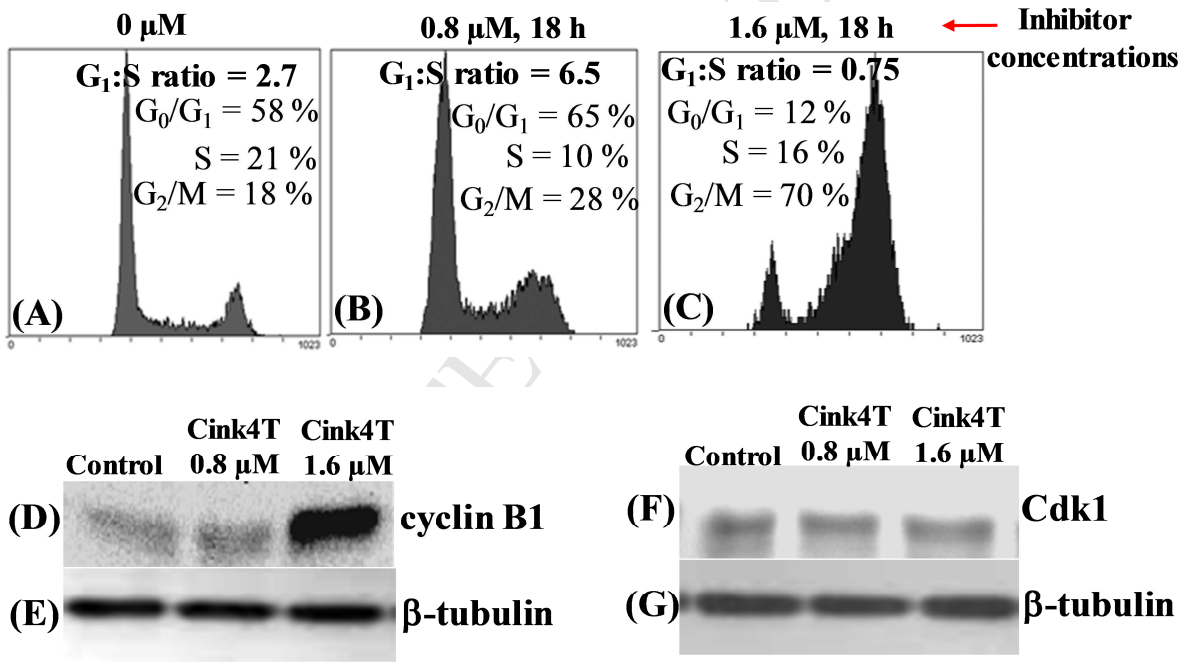

Figure 10. (A) to (C): Cell cycle analyses of A549 (MSC-proficient, pRb^+) cells treated with 1x EC_{50} (0.8 µM) and 2x EC_{50} (1.6 µM)) concentrations of Cink4T. The percentage of cells at each phase of the cell cycle (G_0/G_1; S; G_2/M), at increasing concentrations of Cink4T, are shown. (D) to (G): Western blot analysis of proteins from untreated cells (i.e. Control) and A459 cells treated with 1x EC_{50} and 2x EC_{50} concentrations of Cink4T for 18 h, using antibodies to Cdk1 (CR-UK, Cat # V152), cyclin B1 (Santa Cruz Biotechnology, Cat # sc-98) and β-tubulin (Santa Cruz Biotechnology, Cat # sc-5286). The β-tubulin blots were used as loading controls. An appropriate HRP-conjugated secondary antibody was used to detect the different proteins.

2.12. Mimosine-synchronized MSC-proficient, pRb-positive A549 NSCLC cells at G_1/S, when released in the presence in the presence of Cink4T, undergoes arrest at G_2/M. Mimosine, a non-protein amino acid, inhibits DNA polymerase α in eukaryotic cells which results in a block at the G_1/S boundary of the cell cycle [71]. Since the function of the Cdk4 enzyme is crucial while cells progress through the early G_1 (i.e. G_0/G_1) phase of the cell cycle we hypothesized that if Cink4T selectively inhibits Cdk4 and not Cdk2, it would not affect the progression of cells which have already passed early G_1 and are blocked at the G_1/S boundary. If Cink4T were to be tubulin inhibitor, the cells should progress from G_1/S and get arrested at G_2/M. Studies on the effect of Cink4T on mimosine-treated/blocked cells were performed in order to test these hypotheses.

A549 cells were blocked with mimosine for 32 h and then released in the presence of fresh medium or fresh medium that contained Cink4T. The samples were evaluated by cell cycle analysis after release from block at the 18 h time point. When released in fresh medium, cells re-entered the cell cycle (compare Figures 11A and 11B). At an 1x EC_{50} (0.8 µM) concentration of Cink4T, cells also re-entered the cell cycle but underwent a partial arrest at G_2/M (i.e. 35% cells at G_2/M; Figure 11C). However, cells treated with 2x EC_{50} (1.6 µM) concentration of Cink4T were arrested more profoundly at G_2/M (i.e. 68% cells were at G_2/M; Figure 11D). These results again suggest that there is another protein at G_2/M which Cink4T targets. From our results from the *in vitro* kinase assays (Table 2), we ruled out the involvement of Cdk1 which acts at G_2/M phase of the cell cycle. From our tubulin polymerization results (Figures 2 and 3), we suggest that the target protein must be tubulin.

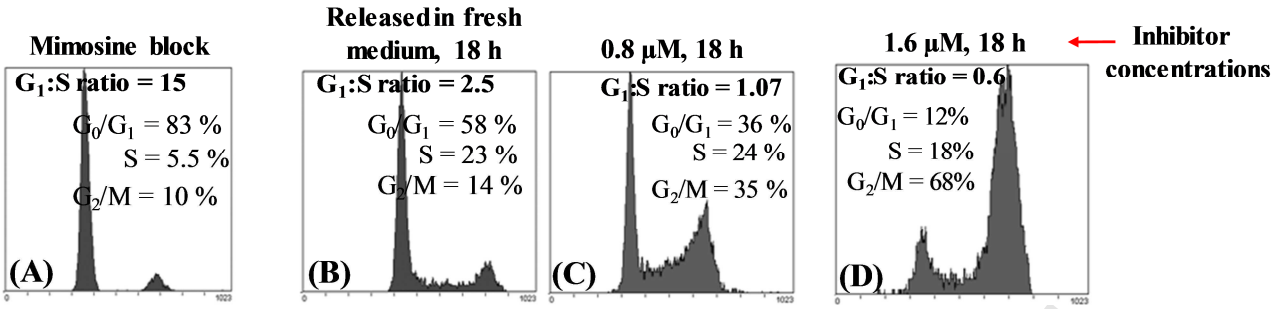

Figure 11. Cell cycle analyses shows that Cink4T does not prevent the re-entry of mimosine-blocked A549 cells from late G_1 (i.e. G_1/S), where Cdk2 acts, into the cell cycle. (A) A549 cells blocked with 200 µM mimosine for 32 h; (B) Mimosine-blocked cells released into fresh medium for 18 h; (C) Mimosine-blocked cells released into fresh medium in the presence of 1x EC_{50} concentration of Cink4T for 18 h; (D) Mimosine-blocked cells released in the presence of 2x EC_{50} concentration of Cink4T for 18 h.

3. Conclusions

Virtual screening of more than 13 million compounds in the drug-like subset of the ZINC13 database, using two relatively weak inhibitors of Cdk4 which also inhibited tubulin polymerization has revealed seven unique scaffolds that possibly inhibit simultaneously both Cdk4 enzyme and tubulin polymerization. We have explored only one of the scaffolds that contains a quinazolinone nucleus. A 59-compound library of quinazolinone derivatives was synthesized on the basis of this virtual screen. It was significant that four compounds were identified in the synthetic library which inhibited Cdk4, one of them (Cink4T) being quite a potent inhibitor of Cdk4 (IC_{50}, 0.47 µM), relative to CA224 (IC_{50}, 6.2 µM [25]) and BPT (IC_{50}, 10 µM [26]) which had been reported earlier. However, like CA224 and BPT, all four compounds inhibited tubulin polymerization to different extents, Cink4T being the most potent.

The results presented here have further established that virtual screens can be extremely useful tools in drug discovery. They may also have significant implications in the design of novel anticancer agents that simultaneously inhibit two crucial targets of the cancer cell division cycle, i.e. Cdk4-cyclin D1 and tubulin polymerization. Continuation of such studies

is likely to lead to the development of novel candidates, with improved potencies, for clinical development.

4. Experimental

4.1. Materials & Methods

Chemicals & solvents used for the synthesis were purchased from Spectrochem, Hi-Media, Acros Organics, Sigma Aldrich and Rankem. Reactions were conducted in dried flask under open air and are monitored using pre-coated silica gel aluminum plates (Merck) under UV light. Final compounds were purified by column chromatography using Merck silica gel (60-100 mesh). Carbon (^{13}C) and Proton (^{1}H) nuclear magnetic resonance (NMR) spectra were recorded on JEOL 400 MHz or Bruker 300 MHz instruments using dimethyl sulfoxide (DMSO-d_6) solvent and tetramethylsilane (TMS) as an internal standard. (^{13}C NMR DMSO: δ 39.5, TMS: δ 0.00 ppm and ^{1}H NMR: DMSO δ 2.5 ppm).

Recombinant protein kinase Cdk4-cyclin D1 (#0142-0143-1), Cdk2-cyclin A2 (#0050-0054-1), Cdk1-cyclin B1 (#0134-0135-1) and Cdk9-cyclin T1 (#0371-0375-1), C-terminal fragment of pRb (RBCTF; #0040-0000-6), RBER CHKtide (#0581-0000-5) were purchased from ProQinase, Germany. The pRb-GST fusion protein (RB796-GST; #SC-4112) was bought from Santacruz Biotech. ADP-Glo kinase detection kit was from Promega (#V9101) and the tubulin polymerization assay kit from Cytoskeleton, (#BK011P).

Propidium iodide (#81845 and #P4170), DMSO (#D8418), bovine serum albumin (BSA; #B4287), DNase-free ribonuclease (# R5503) were purchased from Sigma. 1,4-dithiothreitol was from Melford (#MB1015), and palbociclib (PD-0332991) as control Cdk4 inhibitor, was obtained from Selleck (#1116-SEL).

The cancer cell lines were bought from ATCC: A459 (# CCL-185), Calu1 (# HBT-54), MDA-MB-468 (# HTB-132), and T47D (# HTB-133). They were maintained in RPMI1640 (Sigma #R0883) supplemented with 10% FBS (Gibco, #1704362) and with L-glutamine (Gibco, #25030-024). TrypLE express was bought from Gibco (#12604-021), Pluronic F68 from Gibco (#24040-032), Dulbeco's phosphate buffered saline without calcium and magnesium from Gibco (#14190-094), Lookout mycoplasma PCR kit from Sigma (#MP0035), and 96-well flat-bottomed white polystyrene plates from Corning (#3912).

Statistical Analyses: Data from experiments were analyzed by Microsoft Excel 2010 or GraphPad Prism. Student's t tests were performed to determine IC_{50} and EC_{50} values, using Excel.

***4.2. General procedure for synthesis of benzaldehydes required for the preparation of compounds 35-72*:**

Various substituted anilines were dissolved in glacial acetic acid at 0 °C, to this was added over 30 min choloroacetylchloride (2 equivalents). The reaction mixture was brought to room temperature and stirred overnight. Saturated sodium bicarbonate solution was added till complete neutralization. The resulting precipitate was filtered off and washed with n-hexane and dried. The resultant product was used further without any purification. Either of 3-hydroxy benzaldehyde, 4-hydroxy benzaldehyde, vanillin or isovanillin (1 equivalent) was dissolved in acetone and potassium carbonate (2 equivalents) was added. Then corresponding substituted acetamide was mixed to the stirring solution. Finally, potassium iodide (1.5 equivalent) was added. The reaction mixture was refluxed for 8-10 hrs. After completion of reaction, the resultant mixture was concentrated and treated with water and extracted with ethyl acetate (3 x 20 mL). The organic layers were combined and treated with brine and dried

over sodium sulfate and concentrated. The crude mixture was purified over silica gel (60-120) using petroleum ether: ethyl acetate (9:1).

4.3. General procedure for the synthesis of the newly synthesized compounds 35-72:

To the stirring solution of antranilamide (4.1 equivalents) in dimethylformamide, sodium acetate (2 equivalents) was added. After stirring for 10 min appropriate benzaldehyde derivative (1 equivalent) and iodine (2 equivalents) were added. The reaction mixture was heated at 70-80 °C for 20-24 hrs. Then reaction mixture was poured on to crushed-ice. The resulting mixture was treated with sodium thiosulphate (10% w/v in water) to reduce the remaining iodine. The precipitate was filtered off and washed with n-hexane: ethyl acetate (50:50).

4.4. Spectroscopic data for the newly synthesized compounds 35-72 (for spectra, see Supporting Information)

*4.4.1. N-cyclohexyl-2-[4-(4-oxo-3,4-dihydroquinazolin-2-yl)phenoxy] acetamide (**35**):* White powder, 1.214 g (yield 87.5%)**;** mp: 264-267 °C**;** ^{1}H-NMR (400 MHz, DMSO-d_6) δ 1.20 (d, *J* = 10.4 Hz, 4H, C$\underline{H}_2$) 1.52 (d, *J* = 11.5 Hz, 1H, C$\underline{H}$), 1.64-1.69 (m, 4H, C$\underline{H}_2$), 2.46 (s, 3H, C$\underline{H}_2$), 4.52 (s, 2H, OC$\underline{H}_2$), 8.11-7.04 (m, 9H, ArH), 12.36 (s, 1H, CO-N$\underline{H}$); ^{13}C-NMR (101 MHz, DMSO-D_6) δ 25.48, 25.68, 32.79, 48.13, 67.45, 115.16, 116.44, 121.25, 126.37, 127.53, 129.98, 131.10, 134.90, 149.49, 160.83, 166.66. HRMS (ESI): m/z $[M+H]^+$ calculated 378.1818, found 378.1819

*4.4.2. 2-[4-(4-oxo-3,4-dihydroquinazolin-2-yl)phenoxy]-N-phenylacetamide (**36**):* White powder, 1.281 g (yield 93.98%); mp: 252-253 °C; ^{1}H NMR (400 MHz, DMSO-d_6) δ 4.81 (s, 2H, OC$\underline{H}_2$), 8.18-7.07(m, 13H, Ar-$\underline{H}$), 10.15 (s, 1H, CO-N$\underline{H}$), 12.43 (s, 1H, CO-N$\underline{H}$). ^{13}C-NMR (101 MHz, DMSO-d_6) δ 67.62, 114.92, 117.64, 120.20, 124.21, 126.37, 128.80, 129.27,

129.98, 133.78, 134.62, 135.12, 138.91, 148.54, 152.35, 158.52, 160.94, 164.23, 166.97. HRMS: (ESI): m/z $[M+H]^+$ Calculated 372.13, Found 372.2.

*4.4.3. N-(4-methylphenyl)-2-[4-(4-oxo-3,4-dihydroquinazolin-2-yl)phenoxy]acetamide (**38**):* White powder, 1.401 g (yield 98%); mp: 248-250 °C; ^{1}H NMR (400 MHz, DMSO-d_6) δ 2.24 (s, 3H, Ar-C$\underline{H}_3$), 4.79 (s, 2H, OC$\underline{H}_2$), 8.18-7.13(m, 12H, Ar-H), 10.08 (s, 1H, CO-N$\underline{H}$), 12.42 (brs., 1H, CO-N$\underline{H}$); ^{13}C-NMR (101 MHz, DMSO-d_6) δ 20.89, 67.52, 115.14, 120.15, 125.87, 126.27, 127.74, 129.57, 129.57, 129.87, 133.16, 135.06, 136.24, 149.33, 162.72, 166.34; HRMS (ESI): m/z [M+H]+ calculated 386.1505, found 386.1501

*4.4.4. N-(3-chlorophenyl)-2-[4-(4-oxo-3,4-dihydroquinazolin-2-yl)phenoxy] acetamide (**40**):* White powder, 1.317 g (yield 92.13%); mp: 252-254 °C; ^{1}H NMR (400 MHz, DMSO-d_6) δ 4.83 (s, 2H, OC$\underline{H}_2$), 8.18-7.14 (m, 12H, Ar-$\underline{H}$), 10.35 (s, 1H, CO-N$\underline{H}$),12.43 (br. s, 1H, CO-N$\underline{H}$); ^{13}C-NMR (101 MHz, DMSO-d_6) δ 67.47, 112.71, 115.19, 115.29, 118.55, 119.63, 121.17, 123.95, 126.02, 126.30, 126.69, 127.77, 127.85, 129.93, 130.96, 133.54, 135.04, 140.25, 149.35, 152.27, 160.79, 162.77, 167.09. HRMS (ESI): m/z $[M+H]^+$ calculated 406.0958, found 406.0951

*4.4.5. N-(4-nitrophenyl)-2-[4-(4-oxo-3,4-dihydroquinazolin-2-yl)phenoxy] acetamide (**41**):* Yellowish orange powder, 0.674 g (yield 87.96%); mp: 151-155 °C; ^{1}H NMR (400 MHz, DMSO-d_6) δ 4.95 (s, 2H, OC$\underline{H}_2$), 8.18-7.17 (m, 12H, Ar-H), 9.86 (s, 1H, CO-N$\underline{H}$), 10.91 (s, 1H, CO-N$\underline{H}$); ^{13}C-NMR (101 MHz, DMSO-d_6) δ 67.44, 115.69, 119.35, 125.73, 130.56, 132.55, 143.29, 144.82, 163.23, 167.39, 191.95. HRMS (ESI): m/z $[M+H]^+$ calculated 417.1199, found 417.1198

*4.4.6. N-(4-ethoxyphenyl)-2-[4-(4-oxo-3,4-dihydroquinazolin-2-yl)phenoxy] acetamide (**42**):* White powder, 0.707 g (yield 92.66%); mp: 102-104 °C; ^{1}H NMR (400 MHz, DMSO-d_6) δ 1.29 (t, J = 6.85 Hz, 3H, C$\underline{H}_3$), 3.96 (q, J = 6.85 Hz, 2H, OC$\underline{H}_2$), 4.79 (s, 2H, OC$\underline{H}_2$), 7.88-

6.86 (m, 12H, Ar-H), 9.86 (s, 1H, CO-NH), 10.01 (s, 1H, CO-NH); ^{13}C-NMR (101 MHz, DMSO-d_6) δ 14.7, 63.11, 114.40, 115.22, 121.34, 130.11, 131.28, 131.78, 162.80, 165.38, 191.38. HRMS (ESI): m/z $[M+H]^+$ calculated 416.161, found 416.1605

*4.4.7. N-(naphthalen-2-yl)-2-[4-(4-oxo-3,4-dihydroquinazolin-2-yl)phenoxy] acetamide (**45**):* Light brown powder, 1.22 g (yield 83.5%); mp: 190-192 °C; ^{1}H NMR (400 MHz, DMSO-d_6) δ 4.89 (s, 2H, OCH$_2$), 8.26 - 7.06 (m, 15H, Ar-H), 10.37 (s, 1H, CO-NH), 12.44 (br. s., 1H, CO-NH); ^{13}C-NMR (101 MHz, DMSO-d_6) δ 67.62, 115.26, 116.42, 120.75, 121.24, 125.38, 126.00, 126.37, 126.76, 127.04, 127.89, 128.97, 129.99, 130.48, 133.84, 135.13, 136.47, 149.43, 152.46, 160.82, 162.83, 166.69. HRMS (ESI): m/z $[M+H]^+$ calculated 422.1505, found 422.1499

*4.4.8. N-(naphthalen-1-yl)-2-[4-(4-oxo-3,4-dihydroquinazolin-2-yl)phenoxy] acetamide (**46**):* Cream powder, 0.913 g (yield 59%); mp: 199-201 °C; ^{1}H NMR (400 MHz, DMSO-d_6) δ 5.13 (s, 2H, OCH$_2$), 7.25 -8.00 (m, 13H, Ar-H), 9.89 (s, 1H, CO-NH), 10.23 (s, 1H, CO-NH); ^{13}C-NMR (101 MHz, DMSO-d_6) δ 67.62, 115.79, 122.92, 123.32, 126.09, 126.50, 126.67, 128.66, 130.65, 132.32, 133.27, 134.23, 163.34, 167.33, 191.95. HRMS (ESI): m/z $[M+H]^+$ calculated 422.15, found 422.2

*4.4.9. 2-(4-[4-oxo-3,4-dihydroquinazolin-2-yl)phenoxy]-N-(phenylethyl) acetamide (**48**):* White powder, 1.319 g (yield 91%); mp: 252-253 °C; ^{1}H-NMR (400 MHz, DMSO-d_6) δ 2.46 (q, *J* = 1.8 Hz, 2H, CH$_2$), 2.72 (t, *J* = 7.4 Hz, 2H, CH$_2$), 4.54 (s, 2H, OCH$_2$), 7.04-8.21 (m, 13H, Ar-H), 12.40 (s, 1H, CO-NH); ^{13}C-NMR (101 MHz, DMSO-d_6) δ 35.62, 40.90, 67.47, 115.26, 121.21, 125.93, 126.38, 126.67, 127.72, 128.89, 129.17, 129.97, 135.13, 139.79, 152.40, 160.81, 167.71. HRMS (ESI): m/z $[M+H]^+$ calculated 400. 1661, found 400.1655

*4.4.10. (N-butyl-2-[2-methoxy-4-(4-oxo-3,4-dihydroquinazolin-2-yl)phenoxy] acetamide) (**49**):* Yellowish powder, 0.607 g (yield 88.5%); mp: 185-186 °C; ^{1}H NMR (400 MHz,

DMSO-d_6) δ 0.85 (3 H, t, *J*= 7.24 Hz, C$\underline{H}_3$), 1.25 (2 H, m, C$\underline{H}_2$), 1.39 (2 H, m, C$\underline{H}_2$), 3.11 (2 H, q, *J*=6.58 Hz, C$\underline{H}_2$), 3.89 (3 H, s, OC$\underline{H}_3$), 4.55 (2 H, s, OC$\underline{H}_2$), 7.01-8.07 (m, 7H, Ar-$\underline{H}$), 8.38 (1 H, s, CO-N$\underline{H}$), 12.57 (1 H, br. s, CO-N$\underline{H}$). HRMS (ESI): m/z $[M+H]^+$ calculated 382.1767, found 382.1759.

*4.4.11. 2-[2-methoxy-4-(4-oxo-3,4-dihydroquinazolin-2-yl)phenoxy]-N-(2- methoxy phenyl) acetamide (**50**):* White powder, 0.268 g (yield 84.54%); mp: 253-255 °C; ^{1}H NMR (400 MHz, DMSO-d_6) δ 3.864 (s, 3H, OC$\underline{H}_3$), 3.93 (s, 3H, OC$\underline{H}_3$), 4.803 (s, 2H, OC$\underline{H}_2$), 6.883-8.353 (m, 11H, Ar-$\underline{H}$) 9.286 (s, 1H, CO-N$\underline{H}$), 12.585 (s, 1H, CO-N$\underline{H}$); ^{13}C-NMR (101 MHz, DMSO-d_6) δ 56.48, 68.36, 111.55, 113.83, 120.39, 121.05, 121.71, 124.96, 126.38, 127.10, 134.53, 143.42, 149.13, 149.23, 166.40. HRMS (ESI): m/z $[M+H]^+$ calculated 432.1559, found 432.1559.

*4.4.12. 2-[2-methoxy-4-(4-oxo-3,4-dihydroquinazolin-2-yl)phenoxy]-N-(3-methoxyphenyl) acetamide (**51**):* White powder, 0.263 g (yield 82.96%); mp: 201-203 °C ^{1}H NMR (400 MHz, DMSO-d_6) δ 3.71(s, 3H, OC$\underline{H}_3$), 3.86 (s, 3H, OC$\underline{H}_3$), 4.75 (s, 2H, OC$\underline{H}_2$), 6.85-8.34 (m, 11H, Ar-$\underline{H}$), 9.994 (s, 1H, -CO-N$\underline{H}$), 12.40 (s, 1H, -CO-N$\underline{H}$); ^{13}C-NMR (101 MHz, DMSO-D6) δ 55.80, 56.38, 68.82, 112.37, 113.77, 114.43, 121.70, 122.63, 125.21, 126.39, 126.75, 131.81, 135.13, 147.79, 152.43, 156.11, 166.44.

*4.4.13. 2-[2-methoxy-4-(4-oxo-3,4-dihydroquinazolin-2-yl)phenoxy]-N-(4-methoxyphenyl) acetamide (**52**):* White powder, 1.234 g (yield 77. 91%); mp: 161-163 °C; ^{1}H NMR (400 MHz, DMSO-d_6) δ 3.70 (s, 3H, OC$\underline{H}_3$), 3.86 (s, 3H, OC$\underline{H}_3$),4.80 (s, 2H, OC$\underline{H}_2$), 7.76-6.88 (m, 11H, Ar-$\underline{H}$), 9.83 (s, 1H, -CO-N$\underline{H}$), 10.04 (s, 1H, CO-N$\underline{H}$); ^{13}C-NMR (101 MHz, DMSO-d_6) δ 55.64, 56.11, 68.21, 110.59, 113.28, 114.39, 121.49, 126.07, 130.75, 131.91, 149.80, 153.29, 156.00, 165.78, 191.88. HRMS (ESI): m/z $[M+H]^+$ calculated 432.1559, found 432.1553.

*4.4.14. N-(4-ethoxyphenyl)-2-[2-methoxy-4-(4-oxo-3,4-dihydroquinazolin-2-yl) phenoxy] acetamide (**53**):* White powder, 1.414 g (yield 86.43%); mp: 150-152 °C; ^{1}H NMR (400 MHz, DMSO-d_6) δ 1.300 (t, *J* = 7.2Hz, 3H, C$\underline{H}_3$), 3.856 (s, 3H, OC$\underline{H}_3$), 3.983-3.931 (q, 2H, OC$\underline{H}_2$), 4.792(s, 2H, OC$\underline{H}_2$), 7.530-6.870 (m, 11H, Ar-$\underline{H}$), 9.830 (s, 1H, CO-N$\underline{H}$), 10.015 (s, 1H, CO-N$\underline{H}$); ^{13}C-NMR (101 MHz, DMSO-d_6) δ 15.12, 56.1, 63.56, 68.21, 110.58, 113.28, 114.91, 121.46, 126.08, 130.75, 131.81, 149.80, 153.30, 155.25, 165.76, 191.88. HRMS (ESI): m/z $[M+H]^+$ calculated 446.1716, found 446.1711.

*4.4.15. N-(4-fluorophenyl)-2-[2-methoxy-4-(4-oxo-3, 4-dihydroquinazolin-2-yl)phenoxy] acetamide (**54**):* Yellowish powder, 1.412 g (Yield 91.6%); mp: 135-138 °C; ^{1}H NMR (400 MHz, DMSO-d_6) δ 3.827 (s, 3H, OC$\underline{H}_3$), 4.827 (s, 2H, OC$\underline{H}_2$), 7.626-7.09 (m, 10H, Ar-$\underline{H}$), 9.831, (s, 1H, CO-N$\underline{H}$),10.241 (s, 1H, CO-N$\underline{H}$); ^{13}C-NMR (101 MHz, DMSO-d_6) δ 56.11, 68.10, 110.61, 113.30, 115.75, 115.97, 121.69, 121.77, 126.06, 130.79, 135.22, 149.79, 153.23, 157.50, 159.89, 166.25, 191.89. HRMS (ESI): m/z $[M+H]^+$ calculated 420.136, found 420.1265.

*4.4.16. 2-[2-methoxy-5-(4-oxo-3,4-dihydroquinazolin-2-yl)phenoxy]-N-phenyl acetamide (**58**):* White powder, 1.314 g (yield 89.14%); mp: 227-229 °C; ^{1}H-NMR (400 MHz, DMSO-d_6) δ 3.86 (s, 3H, OC$\underline{H}_3$) 4.78 (s, 2H, OC$\underline{H}_2$), 7.04-8.33 (m, 12H, Ar-$\underline{H}$), 10.08 (s, 1H, CO-N$\underline{H}$), 12.46 (d, J = 52.8 Hz, 1H, CO-N$\underline{H}$); ^{13}C-NMR (101 MHz, DMSO-d_6) δ 56.38, 68.87, 112.38, 113.76, 120.07, 124.25, 126.60, 127.77, 129.36, 134.67, 138.89, 143.42, 147.68, 161.30, 162.74, 167.12. HRMS (ESI): m/z $[M+H]^+$ calculated 402.1454, found 402.1448.

*4.4.17. 2-[2-methoxy-5-(4-oxo-3,4-dihydroquinazolin-2-yl)phenoxy]-N-(2-methoxyphenyl) acetamide (**59**):* White powder, 0.252 g (yield 79.49%); mp 254.5-257 °C; ^{1}H NMR (400 MHz, DMSO-d_6) δ 3.85 (s, 6H, 2 x OC$\underline{H}_3$), 4.818 (s, 2H, OC$\underline{H}_2$), 6.904-8.338 (m, 11H, Ar-$\underline{H}$), 9.275 (s, 1H, CO-N$\underline{H}$), 12.392 (s, 1H, CO-N$\underline{H}$); ^{13}C-NMR (101 MHz, DMSO-d_6) δ 56.49,

56.60, 68.60, 111.81, 112.47, 113.53, 121.06, 123.02, 124.92, 125.24, 126.37, 127.09, 127.84, 135.23, 147.00, 148.95, 152.02, 162.85, 166.74. HRMS (ESI): m/z $[M+H]^+$ calculated 432.1559, found 432.1551.

*4.4.18. 2-[2-methoxy-5-(4-oxo-3,4-dihydroquinazolin-2-yl)phenoxy]-N-(3-methoxyphenyl) acetamide (**60**):* Light brown powder, 0.587 g (yield 92.7%); mp: 114-117 °C; ^{1}H NMR (400 MHz, DMSO-d_6) δ 3.710 (s, 3H, OC<u>H</u>$_3$), 3.904 (s, 3H, OC<u>H</u>$_3$), 4.764 (s, 2H, OC<u>H</u>$_2$), 6.639 - 7.606 (m, 10H, Ar-<u>H</u>), 9.804 (s, 1H, CO-N<u>H</u>), 10.108 (s, 1H, CO-N<u>H</u>); ^{13}C-NMR (101 MHz, DMSO-d_6) δ 55.52, 56.54, 68.27, 105.70, 109.62, 111.68, 112.16, 127.68, 130.18, 140.08, 148.50, 155.20, 160.06, 166.75, 191.83. HRMS (ESI): m/z $[M+H]^+$ calculated 432.1559, found 432.1552.

*4.4.19. 2-[2-methoxy-5-(4-oxo-3,4-dihydroquinazolin-2-yl)phenoxy]-N-(4-methoxyphenyl) acetamide (**61**):* White powder, 1.387 g (yield 87%); mp: 239-240 °C; ^{1}H-NMR (400 MHz, DMSO-D6) 3.68 (s, 3H, OC<u>H</u>$_3$), 3.88 (s, 3H, OC<u>H</u>$_3$), 4.71 (s, 2H, OC<u>H</u>$_2$), 6.86-7.57 (m, 11H, Ar-<u>H</u>), 9.78 (s, 1H, CO-N<u>H</u>), δ 9.97 (s, 1H, CO-N<u>H</u>). HRMS (ESI): m/z $[M+H]^+$ calculated 432.1559, found 432.1554.

*4.4.20. N-(4-ethoxyphenyl)-2-(2-methoxy-5-(4-oxo-3,4-dihydroquinazolin-2-yl)-phenoxy) acetamide (**62**):* White powder, 1.469 g (yield 92.73%); mp: 251-253 °C; ^{1}H NMR (400 MHz, DMSO-d_6) δ 2.72 (t, *J* = 7.09 Hz, 3H, OC<u>H</u>$_3$), 3.33 - 3.39 (m, 2H, OC<u>H</u>$_2$),3.83 (s, 3H, OC<u>H</u>$_3$), 4.58 (s, 2H, OC<u>H</u>$_2$), 6.98-7.49 (m, 11H, Ar-<u>H</u>), 8.03(s, 1H, CO-N<u>H</u>) 9.84 (s, 1H, CO-N<u>H</u>); ^{13}C-NMR (101 MHz, DMSO-d_6) δ 14.68, 55.78, 63.08, 68.33, 111.75, 113.28, 114.40, 121.16, 126.04, 127.26, 131.35, 134.40, 147.32, 151.73, 154.78, 162.43, 166.00. HRMS (ESI): m/z $[M+H]^+$ calculated 446.1716, found 446.1712.

*4.4.21. 2-[2-methoxy-5-(4-oxo-3,4-dihydroquinazolin-2-yl)phenoxy]-N-(2-methylphenyl) acetamide (**63**):* Cream powder, 0.507 g (yield 82.97%); mp: 124-127 °C; Mass (M+1)

Calculated 416.16, found 416.10; ^{1}H NMR (400 MHz, DMSO-D6) δ 2.204 (s, 3H, C<u>H</u>$_3$), 3.87 (s, 3H, OC<u>H</u>$_3$), 4.872 (s, 2H, OC<u>H</u>$_2$), 7.08-7.55 (m, 11H, Ar-<u>H</u>), 9.392 (s, 1H, CO-N<u>H</u>), 9.851 (s, 1H, CO-N<u>H</u>); ^{13}C-NMR (101 MHz, DMSO-D6) δ 18.07, 39.38, 39.59, 39.80, 40.01, 40.22, 40.43, 40.63, 56.21, 68.03, 110.54, 113.65, 124.57, 125.82, 126.18, 126.68, 130.93, 135.86, 149.85, 153.05, 166.18, 192.01.

*4.4.22. N-(2-chlorophenyl)-2-[2-methoxy-5-(4-oxo-3,4-dihydroquinazolin -2-yl)-phenoxy] acetamide (**66**):* Yellowish powder, 1.296 g (yield 81.05%); mp: 227-229 °C; ^{1}H NMR (400 MHz, DMSO-d$_6$) δ 3.867 (s, 3H, OC<u>H</u>$_3$), 4.876 (s, 2H, OC<u>H</u>$_2$), 7.143-8.035 (m, 11H, Ar-<u>H</u>), 9.564 (s, 1H, CO-N<u>H</u>), 12.406 (s, 1H, CO-N<u>H</u>); ^{13}C-NMR (101 MHz, DMSO-d$_6$) δ 56.46, 68.47, 112.40, 113.58, 122.94, 124.32, 125.22, 126.39, 127.80, 128.34, 130.03, 134.57, 135.17, 147.11, 149.37, 152.28, 162.86, 167.32. HRMS (ESI): m/z $[M+H]^+$ calculated 436.1064, found 436.1057

*4.4.23. N-(4-chlorophenyl)-2-[2-methoxy-5-(4-oxo-3,4-dihydroquinazolin-2-yl) phenoxy] acetamide (**67**):* Light brown powder, 0.662 g (yield 82.86%); mp: 229 °C; ^{1}H NMR (400 MHz, DMSO-d$_6$) δ 3.879 (s, 3H, OC<u>H</u>$_3$); 4.820 (s, 2H, OC<u>H</u>$_2$), 8.109-7.71(m, 11H, Ar-<u>H</u>), 10.32 (s, 1H, CO-N<u>H</u>), 12.71 (s, 1H, CO-N<u>H</u>); ^{13}C-NMR (101 MHz, DMSO-d$_6$) δ 56.33, 68.76, 112.37, 113.68, 121.62, 125.14, 126.31, 127.70, 127.78, 129.18, 137.79, 147.64, 167.15. HRMS (ESI): m/z $[M+H]^+$ calculated 436.1064, found 436.1061

*4.4.24. N-(4-fluorophenyl)-2-[2-methoxy-5-(4-oxo-3,4-dihydroquinazolin-2-yl) phenoxy] acetamide (**68**):* White powder, 1.41 g (yield 91.5%); mp: 124-126 °C; ^{1}H NMR (400 MHz, DMSO-d$_6$) δ 3.898 (s, 3H, OC<u>H</u>$_3$); 4.792 (s, 2H, OC<u>H</u>$_2$), 7.810-7.114(m, 10H, Ar-<u>H</u>),9.779 (s, 1H, CO-N<u>H</u>),10.364 (s, 1H, CO-N<u>H</u>), ^{13}C-NMR (101 MHz, DMSO-d$_6$) δ 39.39, 39.59, 39.80, 40.01, 40.22, 40.43, 40.63, 56.44, 68.22, 111.83, 112.33, 118.61, 119.49, 123.93, 127.68,

131.09, 133.95, 140.53, 148.41, 154.80, 167.00, 191.83. HRMS (ESI): m/z $[M+H]^+$ calculated 420.136,found 419.9925.

*4.4.25. 2-(2-methoxy-5-(4-oxo-3,4-dihydroquinazolin-2-yl)phenoxy)-N-(4-nitrophenyl) acetamide (**70**):* Yellowish powder, 0.279 g (yield 85%); mp: 269-272 °C; ^{1}H-NMR (400 MHz, DMSO-d_6) δ 3.86 (s, 3H, OC$\underline{H}_3$), 4.86 (s, 2H, OC$\underline{H}_2$), 7.14- 8.33 (m, 11H, Ar-$\underline{H}$), 10.75 (s, 1H, -CO-N$\underline{H}$), 12.52 (s, 1H, -CO-N$\underline{H}$); ^{13}C-NMR (101 MHz, DMSO-d_6) δ 56.62, 68.68, 112.45, 113.74, 119.73, 122.86, 124.92, 125.59, 134.67, 143.02, 143.41, 145.28, 147.65, 152.51, 168.03. HRMS (ESI): m/z $[M+H]^+$ calculated 447.1305, found 447.1275.

4.5. Cyclin dependent kinase (Cdk) assays (ADP-Glo luminescence). The ADP-Glo cyclin dependent kinase (Cdk) assays were performed as per manufacturer's instructions. The ADP-Glo kinase assay is a two-step reaction which measures kinase activity by quantifying the amount of ADP formed during a kinase reaction. Step 1: After the kinase reaction, an equal volume of ADP-Glo™ Reagent is added to terminate the kinase reaction and deplete the remaining ATP. Step 1: A Kinase Detection Reagent is added to convert ADP to ATP allowing the newly synthesized ATP to be measured using a luciferase/luciferin (Ultra-Glo luciferase) reaction. For initiation of kinase reactions, inhibitors (10x concentrations), enzyme (200 ng per reaction), 2.5x ultrapure ATP and substrate (125 µM and 25 µg respectively) were diluted in 4x kinase buffer with 4% DMSO (40 mM Tris, 20mM $MgCl_2$, 0.1 mg/mL BSA, 50 µM DTT, with 3 mM $MnCl_2$ as cofactor). 5µL 10x inhibitors prepared in 1x kinase buffer containing 5% DMSO were added to wells of a 96-well white microtiter plate followed by addition of 10 µL (0.05 µg/µL) of Cdk enzyme and10 µL of ATP/substrate mix. Reaction mixtures were mixed on a shaker and the plate was incubated for 1h at 21ºC (room temperature). ADP-Glo reagent (25 µL) was added to the reaction mixture and plate was incubated for 40 min at 21ºC. 50 µL of kinase detection reagent was added and the plate was

further incubated for another 40 min at 21ºC. After completion of incubation, the plate was read on a plate reader (Fluo Star Omega, Germany) on luminescence mode (measurement time 1 sec, cycle time 60 sec, number of cycles 40). Relative luminescence counts were determined and data was computed in Excel or GraphPad Prism for graphical representation. The enzyme inhibition was plotted using sigmoidal curve (4 parameter variable slope equation) and half inhibitory concentration (IC_{50}) values were analysed statistically using Graph-Pad Prism Software (Version 6.0). The IC_{50} values for Cdk4 inhibition were determined by fitting a non-linear curve of uninhibited fraction against incubation concentration of the inhibitors, using the following four-parameter model (Hill equation): $y = 1 - (\text{Bottom} + (\text{Top} - \text{Bottom})/(1 + (\text{IC50/x})\text{^s}))$, where 'Top' denotes maximum inhibited fraction, 'Bottom' denotes minimum inhibited fraction, 'S' is slope factor, 'x', inhibitor concentration, and 'y' denotes the uninhibited fraction. The parameters 'Top' and 'Bottom' were limited between 0 and 1 by the GraphPad software. To identify potential candidates that inhibit Cdk4 enzyme, a quinazolinone compound library (consisting of ~60 compounds) was initially screened at a single point concertation (10 µM). The potential hits identified from the initial screen were further used for the determination of dose response studies.

4.6. Cell proliferation assay using the propidium iodide (PI) dye. The compounds showing inhibition in Cdk4 enzyme biochemical assay were further tested for their ability to inhibit cancer cell growth. The four cancer cell lines that were used were: (i) NSCLC A549 (MSC-proficient, pRb^+, $p53^+$), (ii) NSCLC Calu-1 (MSC-deficient, pRb^+, p53-null), (iii) breast cancer cells MDA-MB-468 (MSC-deficient, pRb-null, p53mut) and (iv) breast cancer cells T47D (MSC-deficient, pRb^+, p53mut). All cell lines were chosen for their relative resistance to chemotherapeutic agents. Pablociclib, a potent Cdk4 inhibitor, was included as a positive control. The genotypes within brackets indicate the status of the retinoblastoma

protein pRb and p53 (TP53), two tumor suppressor proteins. The cell lines were maintained at 37ºC in 5% CO_2 in RPMI-1640 medium, supplemented with 10% FBS. Cells, (10,000 cells per well) from different cell lines, were seeded in 96-well plates in complete growth medium and incubated for 24 h. 10 mM stock solutions of compounds in DMSO were serially diluted in medium, without serum. 20 µL of compounds were added into the wells of the microtiter plates, in triplicate, while equivalent amounts of DMSO were added to the control wells. The contents of the wells were mixed gently and incubated further for 72 h. After exposure to compound, wells were washed three times with PBS and 200 µL of an aqueous PI solution (7 µg/mL) was added. As PI dye only penetrates through leaky or lysed cell membranes, DNA of dead cells will be stained and measured, whereas live cells will not be stained. To measure the proportion of live cells, cells were permeabilized by freezing the plates, resulting in death of all cells. After thawing of the plates, fluorescence was measured using the BMG Labtech fluorescence reader (excitation, 530 nm; emission, 620 nm). Percentage of growth inhibition was expressed as treated/control x 100 (%T/C).

4.7. Flow cytometric analyses. The untreated (control) and treated (with Cink4T) cells were harvested by trypsinization, washed once with PBS, and then fixed in 70% chilled (−20°C) ethanol for a minimum of 1 h. After the fixation step, cells were centrifuged for 5 min at 3000g at room temperature, and the pellet was then suspended in PBS containing 50 µg/mL propidium iodide and 0.5 mg/mL DNase-free ribonuclease. The cells were stained for 1 h in the dark at 4°C. Cell cycle analysis was performed on a Beckman Coulter (Epics Altra) fluorescence-activated cell sorter. In order to gate all of the events that represent single cells and to exclude cell doublets or cell clumps, the following analyses were performed on the samples. Cytograms of propidium iodide fluorescence peak signal versus integrated fluorescence or the linear signal were plotted. All data points on the straight line were isolated in a single gate, and the gated data were further used for plotting a histogram that represents a

complete cell cycle. The total number of events was not allowed to exceed 200 events/second. Data acquisition was stopped after a minimum of 10,000 events had been collected.

4.8. Cell synchronization for flow cytometric analysis. The cell synchronization of T47D and Calu-1 cells at G_0/G_1 was achieved by incubating cells in medium containing 0.1% FBS for 24 h and then the synchronised cells were released in the presence or absence of Cink4T. To synchronize A549 cells at G_2/M, mimosine (Calbiochem) was prepared as a 10 mM stock solution in 100% DMSO and then added to cultures to obtain a final concentration of 200 mM; cells were incubated at 37°C for 32 h. Cells were washed and incubated in fresh medium in the absence or presence of compounds. After fixation the samples were analysed by flow cytometry. The detail procedure for fixation and flow cytometric analysis has been described previously [25, 26, 48].

4.9. Tubulin polymerization assay *in vitro*. Standard polymerization assay was carried out to determine whether a Cdk4 inhibitor was a potential inhibitor or enhancer of tubulin polymerization, in the presence of 2 mg/mL tubulin, 80 mM PIPES, pH 6.6, 2 mM $MgCl_2$, 0.5 mM EGTA, 1 mM GTP and 15% Glycerol. 5 µL of control buffer and 10x stock solutions of inhibitors, paclitaxel (as enhancer control) and $CaCl_2$ (as inhibitor control) was added in duplicates to the 96 half-well black plate provided by the kit manufacturer. After quick addition of test compounds to wells, plate was placed in the plate reader to warm up the contents at 37ºC for no more than a minute, to prevent evaporation of solution in wells. Immediately, 50 µL of tubulin reaction pre-mix solution, which had been placed on ice, was carefully added to wells to avoid formation of bubbles. The reaction buffer contained enough Buffer 1 (205 µL), tubulin glycerol buffer (150 µL), GTP stock solution (4.4 µL) and Tubulin stock solution (85 µL). Relative fluorescence units (RFU) were measured at 360 (excitation)

and 460 (emission) for 60 min and the trend of the reaction was compared with paclitaxel as an enhancer and $CaCl_2$ as destabilizing agent.

4.10. Molecular modeling of Cink4T with Cdk4 and tubulin. Hybrid-Cdk4 model based on the X-ray crystal structure of Cdk4 (PDB:2W96)[72] published by Shafiq et al [73] and X-ray crystal structure of Cdk2 (PDB:1FIN) [74] were employed to study the binding mode of Cink4T with Cdk4 and Cdk2, respectively. Proteins were prepared for molecular docking simulation through pdb2pqr web-server [75]. Both proteins were superimposed on 1GII [50] and co-ordinates were rewritten using Chimera. This enabled the location of active sites of 2W96 and 1FIN using the co-ordinates of 1GII-cocrystalized ligand. Autodock-4.2 [76] program was used to run the molecular docking simulation. Grid parameter file (.gpf) and Docking parameter files (.dpf) were written using AutoDock Tools (ADT) implemented in MGLTools-1.5.6 [76]. Grid of volume 50x50x50 was constructed using the co-ordinates of co-crystallized ligand (1PU) of 1GII using the option center of the grid as center of the ligand. Grid maps for protein and ligand atom type specified in .gpf file were generated using autogrid-4.2. Cink4T was sketched and prepared for molecular docking simulation through prodrg web-server [77]. Each docking simulation was carried out with 100 runs using autodock-4.2. All the other parameters were kept at default values. Similar protocol was adopted for molecular docking simulation of Cink4T with tubulin. Chains C and D from the X-ray crystal structure of tubulin complexed with colchicine (PDB: 1SA0)[78] were selected for the study. Protein and ligand preparations were done using the pdb2pqr [75] and prodrg [77] web-servers, respectively. Co-ordinates of the co-crystallized ligand (CN2) have been used to construct the grid with the volume of 50x50x50 with the center of the ligand as center of the grid and docking run was kept at 100. Docking analysis were performed through MGLTools-1.5.6. The 3D (3-dimensional) and 2D (2-dimensional) interaction images were created using UCSF Chimera [79] and Ligplot^{+} [80], respectively.

Acknowledgements. The work was supported by funds from UKIERI (BC), UGC (BNS) [184-20/2013(IC)], HEIF-UK (BC) and CYP-Design Ltd (BC). MUMS acknowledge UGC [184-20/2013(IC)] for support of the chemistry aspect of the project and also UGC for award of MANF-JRF fellowship [201516-MANF-2015-17-MAH-60712]. SSJ is thankful for SERB for PDF [PDF/2017/001556]. BNS and VJ acknowledge DST-FIST [SR/FST/CSI-242/2012] for NMR facility at the Birla Institute of Technology, Mesra

References

[1] D.G. Johnson, C.L. Walker, Cyclins and cell cycle checkpoints, Annu. Rev. Pharmacol. Toxicol., 39 (1999) 295-312. https://doi.org/10.1146/annurev.pharmtox.39.1.295

[2] K.L. King, J.A. Cidlowski, Cell cycle regulation and apoptosis, Annu. Rev. Physiol., 60 (1998) 601-617. https://doi.org/10.1146/annurev.physiol.60.1.601

[3] D.O. Morgan, Principles of CDK regulation, Nature, 374 (1995) 131. https://doi.org/10.1038/374131a0

[4] I.R. Hardcastle, B.T. Golding, R.J. Griffin, Designing inhibitors of cyclin-dependent kinases, Annu. Rev. Pharmacol. Toxicol., 42 (2002) 325-348. https://doi.org/10.1146/annurev.pharmtox.42.090601.125940

[5] I. Collins, M.D. Garrett, Targeting the cell division cycle in cancer: CDK and cell cycle checkpoint kinase inhibitors, Curr. Opin. Pharm., 5 (2005) 366-373. https://doi.org/10.1016/j.coph.2005.04.009

[6] R. Roskoski, Cyclin-dependent protein kinase inhibitors including palbociclib as anticancer drugs, Pharmacol. Res., 107 (2016) 249-275. https://doi.org/10.1016/j.phrs.2016.03.012

[7] L. Santo, K.T. Siu, N. Raje, Targeting cyclin-dependent kinases and cell cycle progression in human cancers, Semin. Oncol., 42 (2015) 788-800. https://doi.org/10.1053/j.seminoncol.2015.09.024

[8] A.M. Senderowicz, Flavopiridol: The first cyclin-dependent kinase inhibitor in human clinical trials, Invest. New Drugs, 17 (1999) 313-320. https://doi.org/10.1023/A:1006353008903

[9] J. Veselý, L. Havlíček, M. Strnad, J.J. Blow, A. Donella-Deana, L. Pinna, D.S. Letham, J.-y. Kato, L. Detivaud, S. Leclerc, L. Meijer, Inhibition of cyclin-dependent kinases by purine analogues, Eur. J. Biochem., 224 (1994) 771-786. https://doi.org/10.1111/j.1432-1033.1994.00771.x

[10] W.F. Azevedo, S. Leclerc, L. Meijer, L. Havlicek, M. Strnad, S.-H. Kim, Inhibition of cyclin-dependent kinases by purine analogues, Eur. J. Biochem., 243 (1997) 518-526. https://doi.org/10.1111/j.1432-1033.1997.0518a.x

[11] N.S. Gray, L. Wodicka, A.-M.W.H. Thunnissen, T.C. Norman, S. Kwon, F.H. Espinoza, D.O. Morgan, G. Barnes, S. LeClerc, L. Meijer, S.-H. Kim, D.J. Lockhart, P.G. Schultz, Exploiting chemical libraries, structure, and genomics in the search for kinase inhibitors, Science, 281 (1998) 533. https://doi.org/10.1126/science.281.5376.533

[12] D.W. Zaharevitz, R. Gussio, M. Leost, A.M. Senderowicz, T. Lahusen, C. Kunick, L. Meijer, E.A. Sausville, Discovery and initial characterization of the paullones, a novel class of small-molecule inhibitors of cyclin-dependent kinases, Cancer Res., 59 (1999) 2566.

[13] M. Kitagawa, H. Higashi, I. Takahashi, T. Okabe, H. Ogino, Y. Taya, S. Hishimura, A. Okuyama, A cyclin-dependent kinase inhibitor, butyrolactone I, inhibits phosphorylation of RB protein and cell cycle progression, Oncogene, 9 (1994) 2549-2557.

[14] H.N. Bramson, J. Corona, S.T. Davis, S.H. Dickerson, M. Edelstein, S.V. Frye, R.T. Gampe, P.A. Harris, A. Hassell, W.D. Holmes, R.N. Hunter, K.E. Lackey, B. Lovejoy, M.J. Luzzio, V. Montana, W.J. Rocque, D. Rusnak, L. Shewchuk, J.M. Veal, D.H. Walker, L.F. Kuyper, Oxindole-based inhibitors of cyclin-dependent kinase 2 (cdk2): Design, synthesis, enzymatic activities, and X-ray crystallographic analysis, J. Med. Chem., 44 (2001) 4339-4358. https://doi.org/10.1021/jm010117d

[15] C.J. Helal, M.A. Sanner, C.B. Cooper, T. Gant, M. Adam, J.C. Lucas, Z. Kang, S. Kupchinsky, M.K. Ahlijanian, B. Tate, F.S. Menniti, K. Kelly, M. Peterson, Discovery and SAR of 2-aminothiazole inhibitors of cyclin-dependent kinase 5/p25 as a potential treatment for Alzheimer's disease, Biorg. Med. Chem. Lett., 14 (2004) 5521-5525. https://doi.org/10.1016/j.bmcl.2004.09.006

[16] G. Zhu, S.E. Conner, X. Zhou, C. Shih, T. Li, B.D. Anderson, H.B. Brooks, R.M. Campbell, E. Considine, J.A. Dempsey, M.M. Faul, C. Ogg, B. Patel, R.M. Schultz, C.D. Spencer, B. Teicher, S.A. Watkins, Synthesis, structure−activity relationship, and biological studies of indolocarbazoles as potent cyclin D1-cdk4 Inhibitors, J. Med. Chem., 46 (2003) 2027-2030. https://doi.org/10.1021/jm0256169

[17] S. Wang, C. Meades, G. Wood, A. Osnowski, S. Anderson, R. Yuill, M. Thomas, M. Mezna, W. Jackson, C. Midgley, G. Griffiths, I. Fleming, S. Green, I. McNae, S.-Y. Wu, C. McInnes, D. Zheleva, M.D. Walkinshaw, P.M. Fischer, 2-anilino-4-(thiazol-5-yl)pyrimidine cdk inhibitors: Synthesis, SAR analysis, X-ray crystallography, and biological activity, J. Med. Chem., 47 (2004) 1662-1675. https://doi.org/10.1021/jm0309957

[18] S. Dhillon, Palbociclib: First Global Approval, Drugs, 75 (2015) 543-551. https://doi.org/10.1007/s40265-015-0379-9

[19] D.M. Roll, C.M. Ireland, H.S.M. Lu, J. Clardy, Fascaplysin, an unusual antimicrobial pigment from the marine sponge Fascaplysinopsis sp, J. Org. Chem., 53 (1988) 3276-3278. https://doi.org/10.1021/jo00249a025

[20] R. Soni, L. Muller, P. Furet, J. Schoepfer, C. Stephan, S. Zumstein-Mecker, H. Fretz, B. Chaudhuri, Inhibition of cyclin-dependent kinase 4 (cdk4) by fascaplysin, a marine natural

product, Biochem. Biophys. Res. Commun., 275 (2000) 877-884. https://doi.org/10.1006/bbrc.2000.3349

[21] A. Hörmann, B. Chaudhuri, H. Fretz, DNA binding properties of the marine sponge pigment fascaplysin, Biorg. Med. Chem., 9 (2001) 917-921. https://doi.org/10.1016/S0968-0896(00)00313-8

[22] C. Aubry, A.J. Wilson, P.R. Jenkins, S. Mahale, B. Chaudhuri, J.-D. Maréchal, M.J. Sutcliffe, Design, synthesis and biological activity of new CDK4-specific inhibitors, based on fascaplysin, Org. Biomol. Chem., 4 (2006) 787-801. https://doi.org/10.1039/b518019h

[23] P.R. Jenkins, J. Wilson, D. Emmerson, M.D. Garcia, M.R. Smith, S.J. Gray, R.G. Britton, S. Mahale, B. Chaudhuri, Design, synthesis and biological evaluation of new tryptamine and tetrahydro-β-carboline-based selective inhibitors of CDK4, Biorg. Med. Chem., 16 (2008) 7728-7739. https://doi.org/10.1016/j.bmc.2008.07.002

[24] C. Aubry, A.J. Wilson, D. Emmerson, E. Murphy, Y.Y. Chan, M.P. Dickens, M.D. García, P.R. Jenkins, S. Mahale, B. Chaudhuri, Fascaplysin-inspired diindolyls as selective inhibitors of CDK4/cyclin D1, Biorg. Med. Chem., 17 (2009) 6073-6084. https://doi.org/10.1016/j.bmc.2009.06.070

[25] S. Mahale, S.B. Bharate, S. Manda, P. Joshi, S.S. Bharate, P.R. Jenkins, R.A. Vishwakarma, B. Chaudhuri, Biphenyl-4-carboxylic acid [2-(1H-indol-3-yl)-ethyl]-methylamide (CA224), a nonplanar analogue of fascaplysin, Inhibits cdk4 and tubulin polymerization: evaluation of *in vitro* and *in vivo* Anticancer Activity, J. Med. Chem., 57 (2014) 9658-9672. https://doi.org/10.1021/jm5014743

[26] S. Mahale, S.B. Bharate, S. Manda, P. Joshi, P.R. Jenkins, R.A. Vishwakarma, B. Chaudhuri, Antitumour potential of BPT: a dual inhibitor of cdk4 and tubulin polymerization, Cell Death Dis., 6 (2015) e1743. https://doi.org/10.1038/cddis.2015.96

[27] D. Bates, A. Eastman, Microtubule destabilising agents: far more than just antimitotic anticancer drugs, Br. J. Clin. Pharmacol., 83 (2016) 255-268. https://doi.org/10.1111/bcp.13126

[28] E.A. Perez, Microtubule inhibitors: Differentiating tubulin-inhibiting agents based on mechanisms of action, clinical activity, and resistance, Mol. Cancer Ther., 8 (2009) 2086. https://doi.org/10.1158/1535-7163.MCT-09-0366

[29] P.G. Morris, M.N. Fornier, Microtubule Active Agents: Beyond the Taxane Frontier, Clin. Cancer Res., 14 (2008) 7167. https://doi.org/10.1158/1078-0432.CCR-08-0169

[30] J.A. Hadfield, S. Ducki, N. Hirst, A.T. McGown, Tubulin and microtubules as targets for anticancer drugs, Prog. Cell Cycle Res., 5 (2003) 309-325.

[31] R. Soni, T. O'Reilly, P. Furet, L. Muller, C. Stephan, S. Zumstein-Mecker, H. Fretz, D. Fabbro, B. Chaudhuri, Selective in vivo and in vitro effects of a small molecule inhibitor of cyclin-dependent kinase 4, J. Natl. Cancer Inst., 93 (2001) 436-446. https://doi.org/10.1093/jnci/93.6.436

[32] M. Birk, A. Bürkle, K. Pekari, T. Maier, M. Schmidt, Cell cycle-dependent cytotoxicity and mitotic spindle checkpoint dependency of investigational and approved antimitotic agents, Int. J. Cancer, 130 (2011) 798-807. https://doi.org/10.1002/ijc.26036

[33] I. Hoffmann, Protein kinases involved in mitotic spindle checkpoint regulation, in: P. Kaldis (Ed.) Cell Cycle Regulation, Springer Berlin Heidelberg, Berlin, Heidelberg, 2006, pp. 93-109. https://doi.org/10.1007/b138827

[34] Z. Jin, W.S. El-Deiry, Overview of cell death signaling pathways, Cancer Biol. Ther., 4 (2005) 147-171. https://doi.org/10.4161/cbt.4.2.1508

[35] W.R. Wiedemeyer, I.F. Dunn, S.N. Quayle, J. Zhang, M.G. Chheda, G.P. Dunn, L. Zhuang, J. Rosenbluh, S. Chen, Y. Xiao, G.I. Shapiro, W.C. Hahn, L. Chin, Pattern of retinoblastoma pathway inactivation dictates response to CDK4/6 inhibition in GBM, Proc. Natl. Acad. Sci., 107 (2010) 11501. https://doi.org/10.1073/pnas.1001613107

[36] G.E. Konecny, B. Winterhoff, T. Kolarova, J. Qi, K. Manivong, J. Dering, G. Yang, M. Chalukya, H.-J. Wang, L. Anderson, K.R. Kalli, R.S. Finn, C. Ginther, S. Jones, V.E. Velculescu, D. Riehle, W.A. Cliby, S. Randolph, M. Koehler, L.C. Hartmann, D.J. Slamon, Expression of p16 and retinoblastoma determines response to cdk4/6 Inhibition in ovarian cancer, Clin. Cancer Res., 17 (2011) 1591-1602. https://doi.org/10.1158/1078-0432.CCR-10-2307

[37] L. Connell-Crowley, J.W. Harper, D.W. Goodrich, Cyclin D1/Cdk4 regulates retinoblastoma protein-mediated cell cycle arrest by site-specific phosphorylation, Mol. Biol. Cell, 8 (1997) 287-301. https://doi.org/10.1091/mbc.8.2.287

[38] M. Kitagawa, H. Higashi, H.K. Jung, I. Suzuki-Takahashi, M. Ikeda, K. Tamai, J. Kato, K. Segawa, E. Yoshida, S. Nishimura, Y. Taya, The consensus motif for phosphorylation by cyclin D1-Cdk4 is different from that for phosphorylation by cyclin A/E-Cdk2, EMBO J., 15 (1996) 7060-7069. https://doi.org/10.1002/j.1460-2075.1996.tb01097.x

[39] B. Driscoll, A. T'Ang, Y.-H. Hu, C.L. Yan, Y. Fu, Y. Luo, K.J. Wu, S. Wen, X.-H. Shi, L. Barsky, K. Weinberg, A.L. Murphree, Y.K. Fung, Discovery of a regulatory motif that controls the exposure of specific upstream cyclin-dependent kinase sites that determine both conformation and growth suppressing activity of pRb, J. Biol. Chem., 274 (1999) 9463-9471. https://doi.org/10.1074/jbc.274.14.9463

[40] A. Masuda, K. Maeno, T. Nakagawa, H. Saito, T. Takahashi, Association between mitotic spindle checkpoint Impairment and susceptibility to the induction of apoptosis by anti-microtubule agents in human lung cancers, Am. J. Pathol., 163 (2003) 1109-1116. https://doi.org/10.1016/S0002-9440(10)63470-0

[41] M. Motwani, X.-k. Li, G.K. Schwartz, Flavopiridol, a Cyclin-dependent Kinase Inhibitor, Prevents Spindle Inhibitor-induced Endoreduplication in Human Cancer Cells, Clin. Cancer Res., 6 (2000) 924.

[42] K.E. Hevener, S. Mehboob, P.-C. Su, K. Truong, T. Boci, J. Deng, M. Ghassemi, J.L. Cook, M.E. Johnson, Discovery of a novel and potent class of *F. tularensis* enoyl-reductase (fabi) inhibitors by molecular shape and electrostatic matching, J. Med. Chem., 55 (2012) 268-279. https://doi.org/10.1021/jm201168g

[43] P. Markt, R.K. Petersen, E.N. Flindt, K. Kristiansen, J. Kirchmair, G. Spitzer, S. Distinto, D. Schuster, G. Wolber, C. Laggner, T. Langer, Discovery of novel PPAR ligands by a virtual screening approach based on pharmacophore modeling, 3D shape, and electrostatic similarity screening, J. Med. Chem., 51 (2008) 6303-6317. https://doi.org/10.1021/jm800128k

[44] S.W. Muchmore, A.J. Souers, I. Akritopoulou-Zanze, The use of three-dimensional shape and electrostatic similarity searching in the identification of a melanin-concentrating hormone receptor 1 antagonist, Chem. Biol. Drug Des., 67 (2006) 174-176. https://doi.org/10.1111/j.1747-0285.2006.00341.x

[45] H.J. Wiggers, J.R. Rocha, J. Cheleski, C.A. Montanari, Integration of ligand- and target-based virtual screening for the discovery of cruzain inhibitors, Mol. Inform., 30 (2011) 565-578. https://doi.org/10.1002/minf.201000146

[46] S. Distinto, F. Esposito, J. Kirchmair, M.C. Cardia, M. Gaspari, E. Maccioni, S. Alcaro, P. Markt, G. Wolber, L. Zinzula, E. Tramontano, Identification of HIV-1 reverse transcriptase dual inhibitors by a combined shape-, 2D-fingerprint- and pharmacophore-based virtual screening approach, Eur. J. Med. Chem., 50 (2012) 216-229. https://doi.org/10.1016/j.ejmech.2012.01.056

[47] C. Aubry, P.R. Jenkins, S. Mahale, B. Chaudhuri, J.-D. Maréchal, M.J. Sutcliffe, New fascaplysin-based CDK4-specific inhibitors: design, synthesis and biological activity, Chem. Commun., (2004) 1696-1697. https://doi.org/10.1039/B406076H

[48] S. Mahale, C. Aubry, A. James Wilson, P.R. Jenkins, J.-D. Maréchal, M.J. Sutcliffe, B. Chaudhuri, CA224, a non-planar analogue of fascaplysin, inhibits Cdk4 but not Cdk2 and arrests cells at G0/G1 inhibiting pRB phosphorylation, Biorg. Med. Chem. Lett., 16 (2006) 4272-4278. https://doi.org/10.1016/j.bmcl.2006.05.065

[49] S. Mahale, C. Aubry, P.R. Jenkins, J.-D. Maréchal, M.J. Sutcliffe, B. Chaudhuri, Inhibition of cancer cell growth by cyclin dependent kinase 4 inhibitors synthesized based on the structure of fascaplysin, Bioorg. Chem., 34 (2006) 287-297. https://doi.org/10.1016/j.bioorg.2006.06.004

[50] M. Ikuta, K. Kamata, K. Fukasawa, T. Honma, T. Machida, H. Hirai, I. Suzuki-Takahashi, T. Hayama, S. Nishimura, Crystallographic approach to identification of cyclin-dependent kinase 4 (cdk4)-specific inhibitors by using cdk4 mimic cdk2 protein, J. Biol. Chem., 276 (2001) 27548-27554. https://doi.org/10.1074/jbc.M102060200

[51] Y. Xue, P.T. Wan, P. Hillertz, F. Schweikart, Y. Zhao, L. Wissler, N. Dekker, X-ray Structural Analysis of Tau-Tubulin Kinase 1 and Its Interactions with Small Molecular Inhibitors, ChemMedChem, 8 (2013) 1846-1854. https://doi.org/10.1002/cmdc.201300274

[52] M.U. Mohd Siddique, G.J.P. McCann, V.R. Sonawane, N. Horley, L. Gatchie, P. Joshi, S.B. Bharate, V. Jayaprakash, B.N. Sinha, B. Chaudhuri, Quinazoline derivatives as selective CYP1B1 inhibitors, Eur. J. Med. Chem., 130 (2017) 320-327. https://doi.org/10.1016/j.ejmech.2017.02.032

[53] Z. Dutkiewicz, R. Mikstacka, Structure-based drug design for cytochrome p450 family 1 inhibitors, Bioinorg. Chem. Appl., 2018 (2018) 21. https://doi.org/10.1155/2018/3924608

[54] P.B. Danielson, The Cytochrome P450 Superfamily: Biochemistry, Evolution and Drug Metabolism in Humans, Curr. Drug Metab., 3 (2002) 561-597. https://doi.org/10.2174/1389200023337054

[55] J.H. Lin, A.Y.H. Lu, Inhibition and Induction of Cytochrome P450 and the Clinical Implications, Clin. Pharmacokinet., 35 (1998) 361-390. https://doi.org/10.2165/00003088-199835050-00003

[56] P.D. Adams, X. Li, W.R. Sellers, K.B. Baker, X. Leng, J.W. Harper, Y. Taya, W.G. Kaelin, Retinoblastoma protein contains a C-terminal motif that targets It for phosphorylation by cyclin-cdk complexes, Mol. Cell. Biol., 19 (1999) 1068-1080. https://doi.org/10.1128/MCB.19.2.1068

[57] S. Whittaker, D. Madani, S. Joshi, S.A. Chung, T. Johns, B. Day, M. Khasraw, K.L. McDonald, Combination of palbociclib and radiotherapy for glioblastoma, Cell Death Disc., 3 (2017) 17033. https://doi.org/10.1038/cddiscovery.2017.33

[58] M.L. Shelanski, F. Gaskin, C.R. Cantor, Microtubule assembly in the absence of added nucleotides, Proc. Natl. Acad. Sci., 70 (1973) 765. https://doi.org/10.1073/pnas.70.3.765

[59] J.C. Lee, S.N. Timasheff, In vitro reconstitution of calf brain microtubules: effects of solution variables, Biochemistry, 16 (1977) 1754-1764. https://doi.org/10.1021/bi00627a037

[60] D. Bonne, C. Heuséle, C. Simon, D. Pantaloni, 4',6-Diamidino-2-phenylindole, a fluorescent probe for tubulin and microtubules, J. Biol. Chem., 260 (1985) 2819-2825.

[61] R.J. Owellen, C.A. Hartke, R.M. Dickerson, F.O. Hains, Inhibition of tubulin-microtubule polymerization by drugs of the vinca alkaloid class, Cancer Res., 36 (1976) 1499.

[62] M. Kim, G.D. Kao, Newly identified roles for an old guardian: Profound deficiency of the mitotic spindle checkpoint protein BubR1 leads to early aging and infertility, Cancer Biol. Ther., 4 (2005) 172-173. https://doi.org/10.4161/cbt.4.2.1506

[63] D. Wang, Q. Sun, J. Wu, W. Wang, G. Yao, T. Li, X. Li, L. Li, Y. Zhang, W. Cui, S. Song, A new Prenylated Flavonoid induces G0/G1 arrest and apoptosis through p38/JNK MAPK pathways in Human Hepatocellular Carcinoma cells, Sci. Rep., 7 (2017) 5736. https://doi.org/10.1038/s41598-017-05955-0

[64] Y. Jiang, X. Wang, D. Hu, Furanodienone induces G0/G1 arrest and causes apoptosis via the ROS/MAPKs-mediated caspase-dependent pathway in human colorectal cancer cells: a study in vitro and in vivo, Cell Death Dis., 8 (2017) e2815. https://doi.org/10.1038/cddis.2017.220

[65] L.H. Connell-Crowley, Wade J; Goodrich, David W, Cyclin D1/cdk4 regulates retinoblastoma protein-mediated cell cycle arrest by site-specific phosphorylation, Mol. Biol. Cell, 8 (1997) 287-301. https://doi.org/10.1091/mbc.8.2.287

[66] C.J. Sherr, The Pezcoller lecture: Cancer cell cycles revisited, Cancer Res., 60 (2000) 3689.

[67] X. Li, M. You, Y.-j. Liu, L. Ma, P.-p. Jin, R. Zhou, Z.-X. Zhang, B. Hua, X.-j. Ji, X.-y. Cheng, F. Yin, Y. Chen, W. Yin, Reversal of the apoptotic resistance of non-small-cell lung

carcinoma towards TRAIL by natural product toosendanin, Sci. Rep., 7 (2017) 42748. https://doi.org/10.1038/srep42748

[68] I. Khan, K.R. Garikapati, A.B. Shaik, V.K.K. Makani, A. Rahim, M.A. Shareef, V.G. Reddy, M. Pal-Bhadra, A. Kamal, C.G. Kumar, Design, synthesis and biological evaluation of 1, 4-dihydro indeno[1,2-c] pyrazole linked oxindole analogues as potential anticancer agents targeting tubulin and inducing p53 dependent apoptosis, Eur. J. Med. Chem., 144 (2018) 104-115. https://doi.org/10.1016/j.ejmech.2017.12.010

[69] C.H. Lee, Y.F. Lin, Y.C. Chen, S.M. Wong, S.H. Juan, H.M. Huang, MPT0B169 and MPT0B002, New tubulin Inhibitors, Induce growth Inhibition, G2/M cell cycle arrest, and apoptosis in human colorectal cancer cells, Pharmacology, 102 (2018) 262-271. https://doi.org/10.1159/000492494

[70] Y.-T. Huang, D.-M. Huang, J.-H. Guh, I.L. Chen, C.-C. Tzeng, C.-M. Teng, CIL-102 interacts with microtubule polymerization and causes mitotic arrest following apoptosis in the human prostate cancer PC-3 cell line, J. Biol. Chem., 280 (2005) 2771-2779. https://doi.org/10.1074/jbc.M408850200

[71] S. Kubota, Y. Fukumoto, K. Ishibashi, S. Soeda, S. Kubota, R. Yuki, Y. Nakayama, K. Aoyama, N. Yamaguchi, N. Yamaguchi, Activation of the prereplication complex Is blocked by Mimosine through reactive oxygen species-activated *Ataxia Telangiectasia* mutated (ATM) protein without DNA damage, J. Biol. Chem., 289 (2014) 5730-5746. https://doi.org/10.1074/jbc.M113.546655

[72] P.J. Day, A. Cleasby, I.J. Tickle, M. Reilly, J.E. Coyle, F.P. Holding, R.L. McMenamin, J. Yon, R. Chopra, C. Lengauer, H. Jhoti, Crystal structure of human CDK4 in complex with a D-type cyclin, Proc. Natl. Acad. Sci., 106 (2009) 4166. https://doi.org/10.1073/pnas.0809645106

[73] M.I. Shafiq, T. Steinbrecher, R. Schmid, Fascaplysin as a specific inhibitor for cdk4: Insights from molecular modelling, PLoS One, 7 (2012) e42612. https://doi.org/10.1371/journal.pone.0042612

[74] P.D. Jeffrey, A.A. Russo, K. Polyak, E. Gibbs, J. Hurwitz, J. Massagué, N.P. Pavletich, Mechanism of CDK activation revealed by the structure of a cyclinA-CDK2 complex, Nature, 376 (1995) 313. https://doi.org/10.1038/376313a0

[75] T.J. Dolinsky, J.E. Nielsen, J.A. McCammon, N.A. Baker, PDB2PQR: an automated pipeline for the setup of Poisson–Boltzmann electrostatics calculations, Nucleic Acids Res., 32 (2004) W665-W667. https://doi.org/10.1093/nar/gkh381

[76] G.M. Morris, R. Huey, W. Lindstrom, M.F. Sanner, R.K. Belew, D.S. Goodsell, A.J. Olson, AutoDock4 and AutoDockTools4: Automated docking with selective receptor flexibility, J. Comput. Chem., 30 (2009) 2785-2791. https://doi.org/10.1002/jcc.21256

[77] A.W. Schuttelkopf, D.M.F. van Aalten, PRODRG: a tool for high-throughput crystallography of protein-ligand complexes, Acta Crystallogr. D, 60 (2004) 1355-1363. https://doi.org/10.1107/S0907444904011679

[78] R.B.G. Ravelli, B. Gigant, P.A. Curmi, I. Jourdain, S. Lachkar, A. Sobel, M. Knossow, Insight into tubulin regulation from a complex with colchicine and a stathmin-like domain, Nature, 428 (2004) 198. https://doi.org/10.1038/nature02393

[79] E.F. Pettersen, T.D. Goddard, C.C. Huang, G.S. Couch, D.M. Greenblatt, E.C. Meng, T.E. Ferrin, UCSF Chimera—A visualization system for exploratory research and analysis, J. Comput. Chem., 25 (2004) 1605-1612. https://doi.org/10.1002/jcc.20084

[80] R.A. Laskowski, M.B. Swindells, LigPlot+: Multiple Ligand–Protein Interaction Diagrams for Drug Discovery, J. Chem. Inf. Model., 51 (2011) 2778-2786. https://doi.org/10.1021/ci200227u

Highlights

- Dual inhibitors of Cdk4 & tubulin polymerization (TP) identified employing HTVS
- Quinazolinone scaffold selected from the hits of ligand- → structure-based HTVS
- Four dual inhibitors (**29**, **34**, **40** & **50**) were identified from enumerated library
- Cink4T (**40)**, inhibited Cdk4 & TP with IC_{50} of 0.47 and 0.6 µM, respectively